Finite-size effects in a mean-field kinetically constrained model: dynamical glassiness and quantum criticality

Takahiro Nemoto[1], Vivien Lecomte[2], Shin-ichi Sasa[1] and Frédéric van Wijland[3]

[1] Division of Physics and Astronomy, Graduate School of Science, Kyoto University, Kitashirakawa-Oiwakecho, Sakyo-ku, Kyoto 606-8502, Japan

[2] Laboratoire de Probabilités et Modèles Aléatoires, UMR 7599 CNRS/P7, Université Paris Diderot, 5 rue Thomas Mann, 75205 Paris cedex 13, France

[3] Laboratoire Matière et Systèmes Complexes, UMR 7057 CNRS/P7, Université Paris Diderot, 5 rue Thomas Mann, 75205 Paris cedex 13, France

E-mail: nemoto@ton.scphys.kyoto-u.ac.jp and vivien.lecomte@univ-paris-diderot.fr

Abstract. On the example of a mean-field Fredrickson–Andersen kinetically constrained model, we focus on the known property that equilibrium dynamics take place at a first-order dynamical phase transition point in the space of time realizations. We investigate the finite-size properties of this first-order transition. By discussing and exploiting a mapping of the classical dynamical transition—an argued glassiness signature—to a first-order quantum transition, we show that the quantum analogy can be exploited to extract finite-size properties, which in many respects are similar to those in genuine mean-field quantum systems with a first-order transition. We fully characterize the finite-size properties of the order parameter across the first-order transition.

Contents

1. Introduction

In the realm of the modeling of glassy materials, the idea that metastable states are responsible for the slowing down of the dynamics is an accepted statement. What is however still a matter of debate is whether metastability arises from the wells and valleys of some underlying complex energy landscape, or whether it is dynamically induced by the evolution within the latter energy landscape. Our purpose in this work is not to fuel this debate, but to investigate some refined features of dynamics induced metastability. A family of model systems exhibiting such glassy-like properties is that of kinetically constrained models (KCMs) as presented in the review by Ritort and Sollich [1], or more recently by Garrahan *et al* [2]. When adopting the standpoint of Ruelle, Sinai and Bowen's

thermodynamic formalism [3–5], a Gibbs ensemble construction based on time realizations rather than on instantaneous configurations, it can be seen that the equilibrium dynamics of KCMs take place at a first-order critical point. In a nutshell, trajectories over a large time interval are ordered according to a prescribed value of some meaningful space and time extensive physical observable. The general theory within the framework of Markov dynamics was described by Lecomte *et al* [6], and the idea that this could be relevant to glassy systems was initially put forward by Merolle *et al* [7]. For KCMs, which are lattice systems with discrete degrees of freedom whose evolution rules are encoded in a master equation, the dynamic evolution rules satisfy the detailed balance with respect to an equilibrium distribution for independent degrees of freedom, but the dynamics itself is highly correlated. In KCMs the degrees of freedom are represented by Ising spins or by local occupations numbers (0 or 1), which physically represent local coarse-grained patches of activity. A simple physical observable that we will use to measure the overall activity of a time realization is the number of configuration changes that have taken place over the observation interval. Using the latter quantity to characterize time realizations has revealed that, in KCMs, equilibrium trajectories can be divided into two coexisting groups, those which display a finite activity, and those which are basically frozen in. Within the thermodynamic formalism, this phenomenon is called a dynamical first-order transition, and it can be cast within the same mathematics as that used for ordinary equilibrium (liquid-gas) first-order transition. A full account can be found in Garrahan *et al* [8, 9]. In existing simulations on KCMs that probe this first-order transition scenario, one key difficulty is to overcome the critical point the vicinity of which is responsible for huge numerical difficulties (slowing down, large fluctuations, insufficient numerical sampling). These finite-size effects turn out to be even more serious in realistic atomistic models of glasses [10,11]. Simulations in these systems are necessarily carried out in both finite-time and finite-size. However, while first-order dynamical transitions can be found in systems with few degrees of freedom (such as the simple harmonic oscillator of Whitelam and Garrahan [12] using the time integrated potential energy in lieu of the activity to probe time realizations), those found in KCMs only emerge in the large system size limit. It is therefore crucial to master the behavior of infinite-time but finite-size effects to properly analyze numerical data.

In an effort to address some of these issues, Bodineau and Toninelli [13] proved the existence of a surface tension in the one-dimensional East and Fredrickson–Andersen (FA) models at the coexistence point. In the same vein, an effective interface model was then used by Bodineau, Lecomte and Toninelli [14] to describe finite-size effects in the one-dimensional FA model. A fully solvable model for dynamical first-order phase transitions still hasn't been put forward (unlike second-order phase transitions [15]). It is the purpose of this work to show that, at the price of losing finite-dimensional effects (such as surface tension), the fully connected Fredrickson–Andersen model actually lends itself to such an analysis. This version of the FA model (and its 'bosonic' variant studied in [8, 9]) do not possess a finite-dimensional geometrical structure, but still allow us to take into account the core features of KCMs by using a kinetic constraint where the transition rates for a given site are proportional to the *number* of its occupied neighbors.

In the theory of finite-size corrections in equilibrium first-order transitions is rather recent, and it can be found described in detail in the papers by Borgs and Kotecký [16,17],

though earlier descriptions exist (in particular for the Ising ferromagnet [18]). One of the key messages to be drawn from these works is that the partition function splits in a sum of individual partition functions for each of the pure phases, with the transition occurring when these weights are equal. One may wonder whether this picture applies, in some sense, to our dynamical phase transitions, while there is no corresponding static partition function let alone any static free energy. We would like to present an argument that points in that direction. Let us explain our reasoning. When studying temporal large deviation properties of systems endowed with otherwise equilibrium Markov dynamics, one is left with studying the spectrum of a modified evolution operator which is no longer stochastic. The latter does not conserve probability anymore, for instance. Yet it can nevertheless be symmetrized by means of the standard Darboux transformation [19], thus yielding a Hermitian operator. Studying the dynamical transition is thereby formally identical to studying a quantum first-order transition. By invoking Nelson's trick (as pedagogically described in Parisi's chapter 19 [20]), one can map the quantum mechanical problem back onto a genuine classical and reversible stochastic process. The latter satisfies, as it should, probability conservation and detailed balance. After all, by a series of well-defined mathematical manipulations, dynamical transitions, quantum phase transitions and classical equilibrium phase transitions, are formally equivalent, and so, why bother? If the original classical process displays a dynamical transition, the corresponding quantum system will exhibit a quantum transition and the final classical system as well. However, while the original process and its quantum counterpart are characterized by a smooth dependence in the control parameter driving the phase transition, the resulting final classical process has a built-in singularity (a singular dependence in the control parameter, and long-range effective interactions). Whether and how the standard phenomenology of finite-size scaling applies to this rather nonphysical effective equilibrium process is, in our view, an open question that we shall address in the present work.

Here is how the paper is organized: in sections 2.1 and 2.2, we begin by recalling what the FA model is in its mean-field version and we review the notions of large deviations and dynamical phase transition. Then, in section 2.3, we derive the expression of the free energy for the corresponding classical equilibrium system of the dynamical phase transition point. We also derive the finite-size correction of it with a perturbative approach, which is used for deriving scaling functions in the following sections. In section 2.4, we numerically study the scaling functions around the dynamical transition, and then we derive the analytical expressions corresponding to them in sections 2.5–2.7. For deriving the expressions, we use an ansatz similar to the one used by Borgs and Kotecký for obtaining the finite-size scaling properties in equilibrium first-order transitions [16,17]. From section 3.1, in order to connect our work to recent advances in the realm of quantum phase transitions, we analyze the same quantum mean-field ferromagnet as that studied by Jörg *et al* [21] and later by Bapst and Semerjian [22] to provide, for the latter, a picture for the finite-size scaling functions close to criticality. In sections 3.1 and 3.2, we define the model and review some results in the infinite-size limit. In section 3.3, by using our ansatz, we derive the same expression of the scaling functions in the quantum ferromagnet and numerically check the result. With our ansatz, we can also investigate the scaling factor of the quantum first-order phase transition. In section 3.4, by applying the ansatz to the model, we re-derive the formula for the scaling factor obtained by Bapst and Semerjian in [22]. Note last that the reader will find a table of notations in appendix C.

2. Finite-size scaling for the mean-field FA model

2.1. Definition of the model and settings

Each of the L sites of a fully connected graph is occupied by $n_i = 0$ or 1 particle. A particle may appear at an empty site i, with rate $\frac{c}{L}\sum_{j\neq i} n_j$, and the particle on an occupied site i can disappear with rate $\frac{1-c}{L}\sum_{j\neq i} n_j$. The parameter c takes values between 0 and 1. In those rates, $\frac{1}{L}\sum_{j\neq i} n_j$ represents the number of occupied neighbors to the site i (divided by L); it is the spin-facilitating factor, encoding the kinetic constraint. Because the system is a mean-field model, the transition rate can be written by using only the total occupation number $n \equiv \sum_{i=1}^{L} n_i$. The transition rate for $n \to n \pm 1$ is the sum of the transition rates for each site. That is,

$$w(n \to n+1) = \sum_i (1-n_i)\frac{c}{L}\sum_{j\neq i} n_j = \frac{1}{L}cn(L-n) \tag{1}$$

where n is the kinetic constraint and $L-n$ enumerates the number of empty sites potentially subjected to a creation; and

$$w(n \to n-1) = \sum_i n_i \frac{1-c}{L}\sum_{j\neq i} n_j = \frac{1}{L}(1-c)n(n-1). \tag{2}$$

where $n-1$ is the kinetic constraint and n enumerates the number of occupied sites potentially subjected to an annihilation. The escape rate is written as

$$r(n) = \sum_{n'} w(n \to n') = cn(1-n/L) + (1-c)n(n-1)/L. \tag{3}$$

By convention, we impose $w(n \to n) = 0$. The dynamics for n satisfies the detailed balance condition

$$P_{\mathrm{eq}}(n)w(n \to n') = P_{\mathrm{eq}}(n')w(n' \to n) \quad (\forall\, n, n') \tag{4}$$

with respect to the equilibrium distribution function $P_{\mathrm{eq}}(n)$

$$P_{\mathrm{eq}}(n) = \frac{L!}{n!(L-n)!}\frac{1}{1-(1-c)^L}c^n(1-c)^{L-n}. \tag{5}$$

Note that we completely omit the $n = 0$ state because the system never reaches $n = 0$ whenever the initial distribution function has zero probability for the $n = 0$ state (this state is isolated). The model is thus described by $1 \leqslant n \leqslant L$. The expectation value of n is $\langle n \rangle_{\mathrm{eq}} = cL + O((1-c)^L)$, the variance of n is $\langle (n - \langle n \rangle)^2 \rangle_{\mathrm{eq}} = c(1-c)L + O((1-c)^L)$ and the expectation value of the escape rate is $\langle r \rangle_{\mathrm{eq}} = 2(1-c)c^2 L + O(1)$. The parameter c thus represents the mean density of occupied sites, in the large size limit. We also note that there is a large deviation principle for the probability distribution of the fraction $\rho = n/L$ of occupied sites. The distribution function $L^{-1}P_{\mathrm{eq}}(L\rho)$ for ρ has an asymptotic expression $L^{-1}P_{\mathrm{eq}}(L\rho) \sim \mathrm{e}^{-Lf_{\mathrm{e}}(\rho)}$ at large L, where $f_{\mathrm{e}}(\rho)$ is the large deviation function, and is equal to

$$f_{\mathrm{e}}(\rho) = (1-\rho)\log\frac{1-\rho}{1-c} + \rho\log\frac{\rho}{c}. \tag{6}$$

We will loosely adopt the *free energy* terminology when speaking about the particle number large deviation $f_e(\rho)$ (this applies also to the rest of the paper). The expression in (6) contains an entropic contribution only.

Given a time interval $[0, t]$, the activity K_t is a trajectory-dependent observable defined as the total number of configuration changes the system has undergone up until time t. By using the activity, the free energy in the sense of thermodynamic formalism is defined as

$$\psi(s) = \frac{1}{L} \lim_{t \to \infty} \frac{1}{t} \log \left\langle e^{-sK_t} \right\rangle, \tag{7}$$

where the average is done over trajectories of duration t. In order to distinguish $\psi(s)$ from the equilibrium free energy $f_e(\rho)$, hereafter, we call $\psi(s)$ dynamical free energy. By considering an appropriately biased dynamics, one can show [23, 24] that the dynamical free energy $\psi(s)$ is determined by the largest eigenvalue problem

$$\sum_n \Phi_L(n) W_{n,n'} = L\psi(s) \Phi_L(n'), \tag{8}$$

where W is a $L \times L$ matrix of entries

$$W_{n,n'} = w(n' \to n)e^{-s} - \delta_{n,n'}r(n) \tag{9}$$

and $\Phi_L(n)$ is the left eigenvector corresponding to the largest eigenvalue $L\psi(s)$ of the matrix of entries $W_{n,n'}$. Note that the first term of (9) is purely non-diagonal and corresponds to the actual changes of state in the system, while the last term is purely diagonal and corresponds to the escape rate of configurations. By symmetrizing the matrix, we obtain a mapping to a quantum eigenenergy problem as announced in the *Introduction*. Indeed, if we define a matrix W^{sym} as $W^{sym}_{n,n'} = W_{n,n'}(P_{eq}(n')/P_{eq}(n))^{1/2}$, it is easy to show that W^{sym} is symmetric, by using the detailed balance condition (4). Furthermore, from the definition itself, we have a relationship between $\Phi_L(n)$ and the largest eigenvector $\Phi(n)$ of the symmetrized matrix W^{sym} as $\Phi_L(n)P_{eq}(n)^{1/2} = \Phi(n)$. Thus, the problems of diagonalizing the matrices W and W^{sym} are equivalent. For the ground state energy of a quantum state, a variational principle is well known. By applying it to our case, we obtain a variational expression for the dynamical free energy $\psi(s)$ as

$$L\psi(s) = \max_{\Phi^0 > 0} \frac{\sum_{n,n'} \Phi^0(n) W^{sym}_{n,n'} \Phi^0(n')}{\sum_n \Phi^0(n)^2}. \tag{10}$$

For a generic symmetric matrix W^{sym}, the maximization principle is over non-zero vectors. Here, the optimal vector Φ^0 is unique up to a multiplicative factor, and equal to Φ, whose components are strictly positive. This allows us to restrict the maximization to vectors of strictly positive components as in (10), without loss of generality.

We denote by $K(s)$ the derivative of $-\psi(s)$ with respect to s. From the definition (7) of $\psi(s)$, one has

$$K(s) = \lim_{t \to \infty} \frac{1}{Lt} \frac{\langle K_t e^{-sK_t} \rangle}{\langle e^{-sK_t} \rangle} = -\frac{d\psi}{ds}. \tag{11}$$

The observable $K(s)$ thus describes, in the large time limit, the average activity of trajectories followed by the system, biased towards either active ($s < 0$) or inactive ($s > 0$) regions of the space of possible trajectories.

For several classes of KCMs (including the mean-field FA model considered here), $K(s)$ displays a first-order phase transition in the large system size limit [8, 9]:

$$\lim_{L \to \infty} K(s) \begin{cases} > 0 & \text{for} \quad s \leqslant 0 \text{ (active phase)} \\ = 0 & \text{for} \quad s > 0 \text{ (inactive phase)} \end{cases} \tag{12}$$

The non-biased steady state $s = 0$ lies at the coexistence between the two dynamical phases, characterized by extensive ($K_t = O(L)$) and sub-extensive ($K_t = O(L^0)$) values of the activity in the active and inactive regime respectively. In contrast to the equilibrium statistical physics, the parameter s is not a physical field that can be tuned to induce the phase transition—in the same way as the magnetic field in the Ising model. Indeed, the dynamics directly described by the biased evolution operator (9) does not preserve probability and, to be interpreted, requires for instance one to implement a population dynamics picture [25–27].

However by defining appropriate transition rates, one can build a probability-preserving stochastic dynamics yielding $K(s)$, as extensively discussed in [28, 29] (see also [30]). The result is

$$K(s) = \lim_{t \to \infty} \frac{1}{Lt} \langle K_t \rangle_{\text{st}}^s, \tag{13}$$

where $\langle \cdot \rangle_{\text{st}}^s$ is the stationary average for the dynamics defined by the modified transition rates

$$w_s(n \to n') = w(n \to n') \frac{\Phi_{\text{L}}(n')}{\Phi_{\text{L}}(n)} e^{-s}. \tag{14}$$

The modified dynamics also satisfies detailed balance provided the original one does, with respect to the modified equilibrium distribution

$$P^s(n) = C P_{\text{eq}}(n) \Phi_{\text{L}}(n)^2. \tag{15}$$

Here C is the normalization constant. The advantage of the modified dynamics is that it preserves probability, but the price to pay is that it involves the left eigenvector Φ_{L}, difficult to obtain in general if one wants to render the modified rates explicit.

At $s = 0$, the property $\sum_{n'} W_{n'n} = 0$ ensuring conservation of probability, together with Perron–Frobenius theorem, ensures that $\Phi_{\text{L}}(n) = 1$ is the unique left eigenvector of the matrix $W|_{s=0}$, of maximal eigenvalue 0. At $s \neq 0$, the maximal left eigenvector Φ_{L} takes a less simple form. The free energy is defined as $-\log P^s(n)$ and the free energy difference [28, 29] as

$$\Delta F_s(n) = -2 \log \Phi_{\text{L}}(n). \tag{16}$$

It encodes (see (15)) the modification brought by s to the $s = 0$ equilibrium state P_{eq}. We indeed have $\Delta F_{s=0}(n) = 0$.

We now turn to the study of the dynamical phase transition presented by our model of interest, and to the study of its finite-size scaling. In section 2.2, we focus on the critical point $s_c = s_c(L)$ separating active and inactive dynamical phases, by studying its behavior as L becomes large. It turns out that not only the behavior of the largest eigenvalue, but also of its corresponding eigenvector is essential to the understanding of
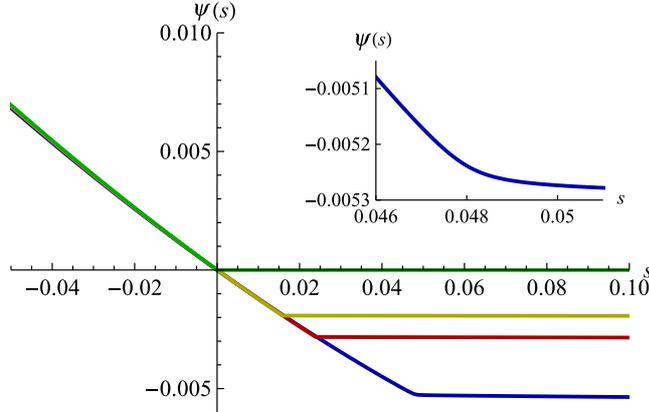
Figure 1. Dynamical free energy $\psi(s)$ for $c = 0.3$, $L = 50$ (blue), $L = 100$ (red), $L = 150$ (yellow) and $L = \infty$ (green). By locating numerically the maximum of $\psi''(s)$, we estimate that s_c is equal to 0.0479... for $L = 50$, 0.02390... for $L = 100$ and 0.01591... for $L = 150$. The value is close to $1/(2Lc(1 - c))$, which takes 0.04762..., 0.02381... and 0.01587... for $L = 50, 100$, and 150, respectively. The $L = \infty$ curve is obtained from the variational formula (58). The inset illustrates the rounding of the cusp due to finite-size, for $L = 50$, in the region of the transition.

the finite-size corrections. In section 2.3 we focus on the exact point of phase coexistence $s = s_c$, and in section 2.4 we determine the generic form of the eigenvector in the vicinity $s \approx s_c$ of the critical point. In section 2.5, we examine how a variational principle can be used to determine this form, and in section 2.6 we actually compute the scaling function for the mean density of occupied sites and for its variance. Last, in section 2.7, we write down the explicit expression of the scaling functions for the two first derivatives of the dynamical free energy $\psi(s)$ encoding the mean and the variance of the activity. We thus fully describe the finite-size behavior of the fluctuation of the activity in our model.

2.2. The dynamical free energy and the upper bound for λ_c

We present in figure 1 the numerical evaluation of the dynamical free energy $\psi(s)$ for $c = 0.3, L = 50, 100, 150$, obtained by solving the largest eigenvalue problem (8) numerically. We observe a remarkable point in each plot where $\psi(s)$ presents a cusp, meaning that $\psi''(s)$ is sharply peaked. We note that the cusp is rounded in the finite-size systems as shown in the inset of figure 1, which becomes sharper as the system size becomes larger. We denote the corresponding s by s_c, and call it the finite-size critical point:

$$s_c \equiv \text{Argmax } \psi''(s). \tag{17}$$

As reported in references [8, 9], s_c deviates from the origin, but goes to zero as $L \to \infty$.

We derive below an upper bound for a scaled critical point

$$\lambda_c = \lim_{L \to \infty} L s_c. \tag{18}$$

By taking $s \to \infty$ in (8), we obtain the asymptotic behavior of $\psi(s)$ at large s

$$\lim_{s \to \infty} \psi(s) = -\frac{1}{L} \min_{n>0} r(n) = -c(L-1)/L^2. \tag{19}$$

Remarking now from (11) that $\psi(s)$ is strictly decreasing, we obtain the inequality

$$\psi(s) > -c(L-1)/L^2, \tag{20}$$

On the other hand, by expanding $\psi(s)$ around $s = 0$, we obtain that

$$\psi(s) = -\langle r \rangle_{\text{eq}} \frac{s}{L} + O(s^2) = -2(1-c)c^2 s + O(s^2). \tag{21}$$

Note that this expansion is valid only in the region around $\lambda = 0$ where $\psi(s)$ remains analytic in the large size limit. To identify this region and define properly its scaling, let us now introduce the rescaled dynamical free energy [13,14]

$$\varphi_L(\lambda) = L\psi(\lambda/L) \tag{22}$$

The transition point s_{c} now defines a critical value $\lambda_{\text{c}} = \lim_{L \to \infty} Ls_c$ where $\varphi_\infty(\lambda) = \lim_{L \to \infty} \varphi_L(\lambda)$ presents a non-analyticity. The previous expansion (21) becomes

$$\varphi_L(\lambda) = -2(1-c)c^2 \lambda + O(\lambda^2/L). \tag{23}$$

Thus one has $\varphi_\infty(\lambda) = -2(1-c)c^2 \lambda$ in the region around $\lambda = 0$ where $\varphi_\infty(\lambda)$ is analytic, while the inequality (20) yields $\varphi_\infty(\lambda) \geqslant -c$ for all values of λ. This implies that $\varphi_\infty(\lambda)$ becomes non-analytic at a point λ_{c} bounded as

$$\lambda_{\text{c}} \leqslant \frac{1}{2c(1-c)} \tag{24}$$

Interestingly, this expression also gives a good approximation for s_{c}: the behavior $s_{\text{c}} \simeq 1/(2Lc(1-c))$ can be checked numerically as displayed in figure 1. In appendix A, building on our results, we shall derive the equality $s_{\text{c}} = 1/(2Lc(1-c)) + O(1/L^2)$.

Remark last that in finite-dimensional FA models, such an approach also yields an upper bound for λ_{c} which however is not the value of λ_{c}, due to the complex interfacial spatial structure of the steady-state around λ_{c} [13,14].

2.3. The free energy difference at $s = s_c$ and the finite-size correction

Let us now study numerical examples of the free energy difference for $s = 0.95s_{\text{c}}$, $s = s_{\text{c}}$ and $s = 1.05\,s_{\text{c}}$: in each subfigure of figure 2 are displayed the free energy difference $\Delta F_s(\rho L)/L$, the original free energy $-\log P_{\text{eq}}(\rho L)/L$, and the modified one $-\log P^s(\rho L)/L$ as functions of the density ρ. For $s = s_{\text{c}}$, one observes that the modified free energy reaches its minimum value at the two values of the density $\rho = n/L$ of occupied sites characterizing the inactive ($\rho \simeq 0$) and the active ($\rho \simeq c$) configurations. This indicates that the first-order phase transition observed along direction s at $s = s_{\text{c}}$ also reflects itself in a first-order coexistence in the density ρ: precisely at $s = s_{\text{c}}$, the two competing phases have the same weight. In this subsection, we consider the analytical expression of the free energy (difference). First, we derive the analytical expression of the free energy $f_s(\rho) \equiv -\lim_{L \to \infty} \frac{1}{L} \log P^s_{\text{eq}}(\rho L)/L$ at $s = s_c$, which describes the distribution

of particle occupation at the transition point in the infinite-size limit. Then, we derive the finite-size correction of these expressions, which will be used for deriving the scaling behavior of this first-order phase transition in the next section.

We start with the eigenvalue equation (8). Since we focus on $s = s_c$, we can set

$$L\psi(s_c) = -c + O(1/L), \tag{25}$$

which leads to

$$\Phi_L(n+1)\frac{cn}{L}(L-n)e^{-s_c} + \Phi_L(n-1)\frac{(1-c)}{L}n(n-1)e^{-s_c}$$
$$-\Phi_L(n)\left[c\frac{n}{L}(L-n) + (1-c)\frac{n}{L}(n-1) - c + O(1/L)\right] = 0. \tag{26}$$

Now, we assume the large deviation principle of $\Phi_L(n)$,

$$\Phi_L(n) = e^{-L\Delta f_{s_c}(n/L)/2}, \tag{27}$$

which defines Δf_{s_c}. By substituting $\Phi_L(n)$ in (26) by the large deviation expression and evaluating the leading order with an assumption of differentiability of $\Delta f_{s_c}(\rho)$, we obtain an equation for determining $\Delta f_{s_c}(\rho)$. That is,

$$e^{-(1/2)\partial\Delta f_{s_c}(\rho)/\partial\rho}c\rho(1-\rho) + e^{(1/2)\partial\Delta f_{s_c}(\rho)/\partial\rho}(1-c)\rho^2 - \left[c\rho(1-\rho) + (1-c)\rho^2\right] = 0. \tag{28}$$

By solving this equation, we obtain two expressions of $\partial\Delta f_{s_c}(\rho)/\partial\rho$ as

$$\partial\Delta f_{s_c}(\rho)/\partial\rho = 0 \tag{29}$$

and

$$\partial\Delta f_{s_c}(\rho)/\partial\rho = -2\log\left[\frac{(1-c)\rho}{c(1-\rho)}\right] = -2\frac{\partial f_e(\rho)}{\partial\rho}, \tag{30}$$

which leads to

$$\Delta f_{s_c}(\rho) = \text{const.} \tag{31}$$

and

$$\Delta f_{s_c}(\rho) = -2f_e(\rho) + \text{const.} \tag{32}$$

We connect these two functions. We call the connecting point ρ_c^∞. By referring the numerical result in figure 2, we conjecture that $\Delta f_{s_c}(\rho)$ becomes

$$\Delta f_{s_c}(\rho) = -2f_e(\rho) + 2f_e(0). \tag{33}$$

for $\rho \leqslant \rho_c^\infty$ and

$$\Delta f_{s_c}(\rho) = -2f_e(\rho_c^\infty) + 2f_e(0). \tag{34}$$

for $\rho > \rho_c^\infty$. Here, ρ_c^∞ is determined from the condition of first-order phase transition expressing here that the inactive ($\rho \simeq 0$) and the active ($\rho \simeq c$) configurations have the same weight

$$f_e(c) + \Delta f_{s_c}(c) = f_e(0) + \Delta f_{s_c}(0), \tag{35}$$
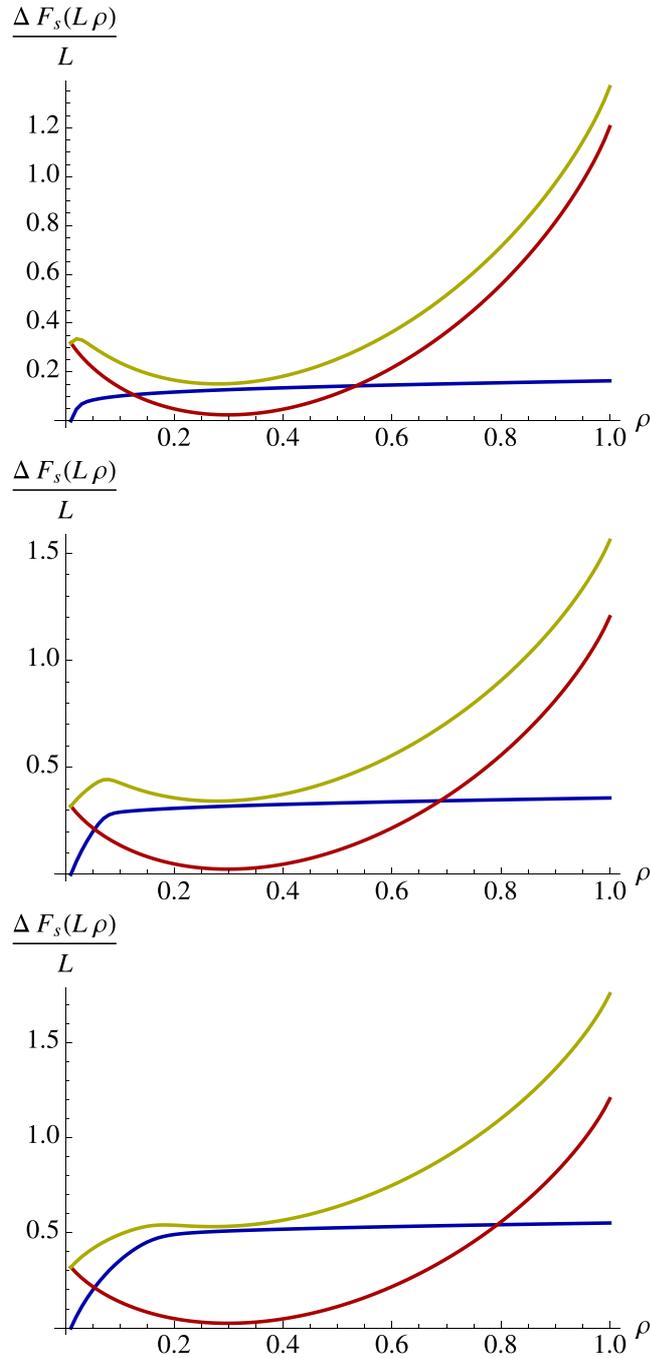
Figure 2. The free energy difference $\Delta F_s(\rho L)/L$ (blue), the original free energy $-\log P_{\mathrm{eq}}(\rho L)/L$ (red) and the modified one $-\log P^s(\rho L)/L = -\log P_{\mathrm{eq}}(\rho L)/L + \Delta F_s(\rho L)/L$ (yellow) for $c = 0.3, L = 100$. We set $s = 0.95 s_{\mathrm{c}}$ (top), $s = s_{\mathrm{c}}$ (middle) and $s = 1.05 s_{\mathrm{c}}$ (bottom). In the $L \to \infty$ limit, those functions converge to analytical forms described by (33), (34) and (36), depicted in figure 4.

Figure 3. Connecting point ρ_c^∞ in the infinite-size limit, as a function of c, obtained from solving (36).

Figure 4. The free energy $f_{\mathrm{e}}(\rho) + \Delta f_{\mathrm{s}_c}(\rho)$ (yellow) for $s = s_c$ and the modifying free energy $\Delta f_{\mathrm{s}_c}(\rho)$ (blue) for $s = s_c$ and the unbiased free energy $f_{\mathrm{e}}(\rho)$ (red). The point $\rho = \rho_{\mathrm{c}}^\infty$ of non-analyticity of the two first functions is provided by the solution of equation (36).

which leads to

$$2 \left[(1 - \rho_{\mathrm{c}}^\infty) \log \frac{1 - \rho_{\mathrm{c}}^\infty}{1 - c} + \rho_{\mathrm{c}}^\infty \log \frac{\rho_{\mathrm{c}}^\infty}{c} \right] = -\log(1 - c). \tag{36}$$
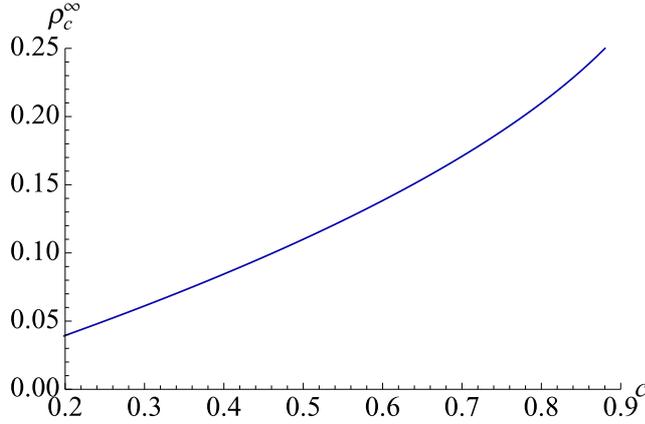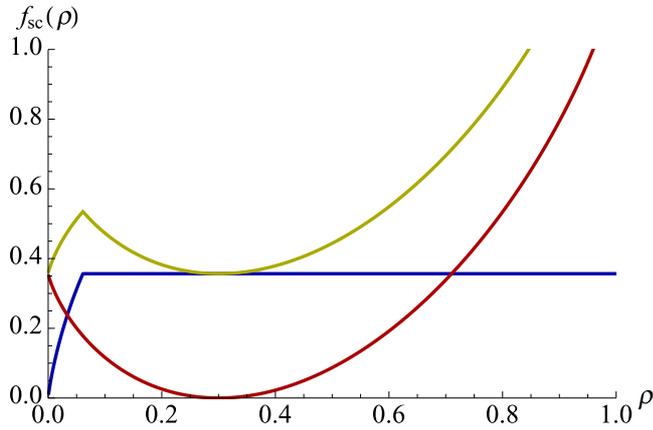
In figure 3, we plot ρ_{c}^∞ as a function of c. Also, in figure 4, we plot the obtained $\Delta f_{\mathrm{s}_c}(\rho)$ with $f_{\mathrm{e}}(\rho) + \Delta f_{\mathrm{s}_c}(\rho)$ and $f_{\mathrm{e}}(\rho)$ for $c = 0.3$. From the figure, we understand that ρ_{c}^∞ is a point of non-analyticity for the free energies: the distribution of the density ρ of occupied sites in the system is naturally divided into two domains, namely, an active ($\rho > \rho_{\mathrm{c}}^\infty$) and an inactive ($\rho < \rho_{\mathrm{c}}^\infty$) domain.

Now, we consider the finite-size correction of the free energy. This will be crucial to understanding the finite-size scaling of the large deviation function, as explained in section 2.6. For this, we conjecture that the kink-like behavior of $\Delta f_{\mathrm{s}_c}(\rho)$ appears faster than $O(1/L)$ as suggested by the numerics presented in figure 7. From this, even for
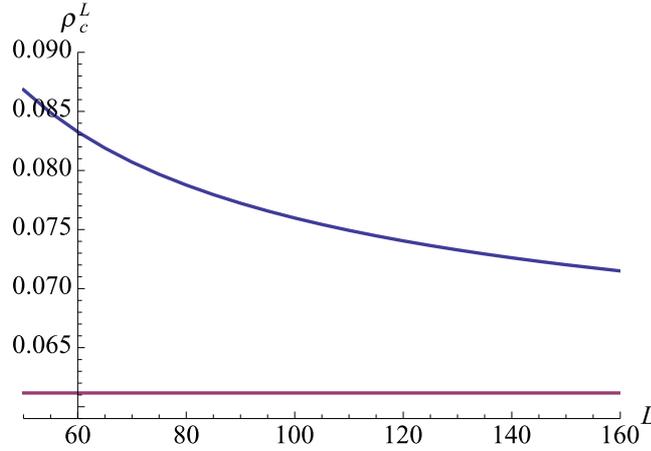
Figure 5. Numerical example illustrating the importance of finite-size corrections for ρ_c^L (in blue), compared to its infinite-size limit ρ_c^∞ (in purple) for $c = 0.3$.

finite-size systems, we can define the active and the inactive regions. We denote the finite-size connecting point by ρ_c^L. Precisely, ρ_c^L is defined as

$$\sum_{n \leqslant n_c^L} P^s(n) = \sum_{n > n_c^L} P^s(n), \tag{37}$$

with the definition of $n_c = \lfloor L\rho_c^L \rfloor$. Here, as shown in what follows, the distribution function $P^s(n)$ itself has a ρ_c^L dependence, so that the equation (37) can give a non-integer value for ρ_c^L. In order to obtain the next order correction of $\Delta f_{s_c}(\rho)$ for each active and inactive region, we use a perturbation analysis. That is, for each region, we assume the following scaling

$$\Phi_{\mathrm{L}}(n) = \exp\left\{-(L/2)\left[\Delta f_{s_c}(n/L) + (1/L)\Delta f_{s_c}^{(1)}(n/L)\right]\right\}. \tag{38}$$

Expanding in powers of L for large L, we obtain the correction $\Delta f_{s_c}^{(1)}(n/L)$ as

$$\Delta f_{s_c}^{(1)}(\rho) = -\log\frac{\rho(1-\rho)}{(c-r)^2} - \frac{\rho(1-2c)}{c(1-c)} + \text{const.} \tag{39}$$

for $\rho \leqslant \rho_c^L$, and

$$\Delta f_{s_c}^{(1)}(\rho) = -2\left[\frac{\rho(2c-1)}{2c(1-c)} - \log\rho\right] + \text{const.} \tag{40}$$

for $\rho > \rho_c^L$. See appendix B for the derivation of these expressions. The two constants in (39) and (40) are determined from the conditions $\Delta f_{s_c}^{(1)}(1/L) = 0$, and $\lim_{\rho\to\rho_c^L}\Delta f_{s_c}^{(1)}(\rho) = \lim_{\rho\to\rho_c^L}\Delta f_{s_c}^{(1)}(\rho)$. We note that the latter constant depends on ρ_c^L. In figure 5, we plot numerical examples of ρ_c^L obtained from (37)–(40) as a function of L, together with the limiting value ρ_c^∞, which is the solution of (36). In figure 6, we compare our finite-size free energy with the numerical results obtained by direct diagonalization, for $c = 0.3$, $s = s_c$, $L = 50, 100, 150$. The agreement of both results improves as L increases.
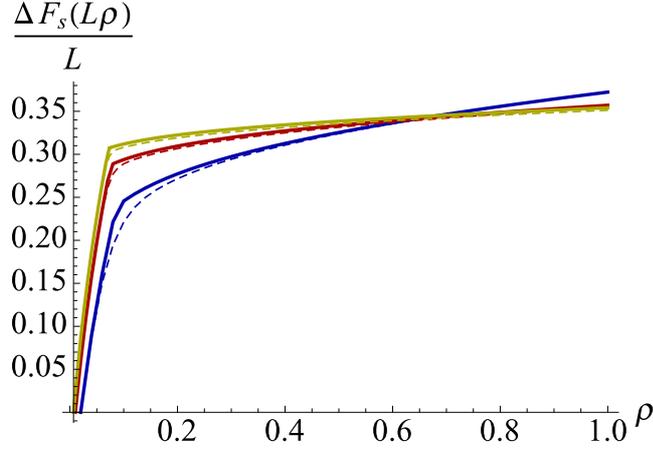
Figure 6. The finite-size correction of the free energy difference for $c = 0.3$, $s = s_c$, $L = 50$ (in blue), $L = 100$ (red) and $L = 150$ (yellow). We plot analytical finite-size free energy difference obtained from (39) and (40) as solid lines. We also plot the exact numerical results as dashed lines. One observes the emergence of the non-analytic point at ρ_c^L as L becomes large.

2.4. Scaling function around $s = s_c$

As seen in the previous section, the system also displays a phase coexistence in the density $\rho = n/L$ of occupied sites, which plays a role similar to the mean magnetization in the Ising model. For the equilibrium ferromagnet model, the scaling functions describing finite-size scaling around the first-order phase transition point have been determined [16, 17]. However, even though our system presents a first-order phase transition, it is not trivial to determine such scaling functions because of the asymmetry of the scalings in the active and inactive phases. In what follows, we study the finite-size scaling behavior in our system.

To do so, we start by considering the statistical properties of the mean occupation n/L. We denote by $\rho(s)$ its expectation value

$$\rho(s) = \sum_n (n/L)P^s(n), \tag{41}$$

and by $\chi(s)$ its variance

$$\chi(s) = L\sum_n (n/L - \rho(s))^2 P^s(n). \tag{42}$$

Examples of these functions are shown in figure 7, and the latter illustrates how the first-order transition materializes around $s = s_c$.

One observes in particular that the width of the first-order coexistence region shrinks as the system size L becomes large. To estimate this dependence in L, we define a scaling ratio κ as

$$\kappa = -\partial\rho(s)/\partial s|_{s=s_c}, \tag{43}$$

which is inversely proportional to the width of the first-order coexistence region, and diverges as $L \to \infty$. The logarithm of κ for various values c is represented as a function of L in figure 8.
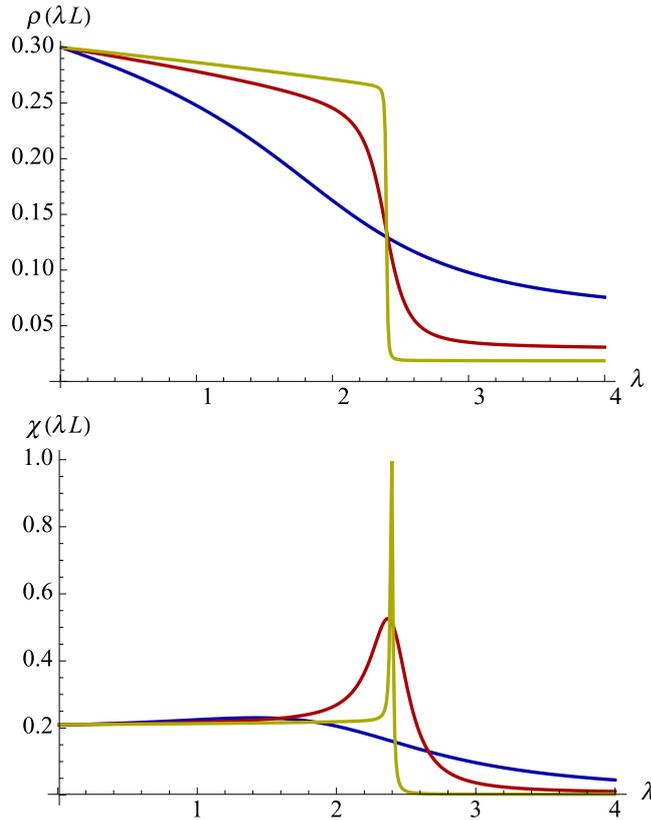
Figure 7. The expectation value $\rho(\lambda L)$ (41) (top) and the variance (42) $\chi(\lambda L)$ (bottom) of the mean occupation n/L in the s-modified equilibrium state, plotted as a function of the rescaled variable $\lambda = s/L$. We set $c = 0.3$ and $L = 20$ (blue), $L = 40$ (red) and $L = 60$ (yellow). The position of the peak of $\chi(s)$ defines the value of s_c, which appears on the graphs as a function of λ at a value close to the critical $\lambda_\mathrm{c} = 1/(2c(1-c))$ derived in section 2.2. For example, the peak occurs approximately at $\lambda = 2.398...$ for $L = 60$, which is close to the corresponding $\lambda_\mathrm{c} \simeq 2.381....$

We find that these logarithms are increasing linear functions of L. It indicates that the width of the first-order coexistence region (illustrated in figure 7) shrinks exponentially with the system size L.

Next, we search for the scaling functions of $\rho(s)$ and $\chi(s)$ in the coexistence region. For this purpose, we introduce a scaling variable x as

$$x = \kappa(s - s_\mathrm{c}). \tag{44}$$

Correspondingly, the rescaled expectation value and variance are defined as

$$\tilde{\rho}(x) = \rho(x\kappa^{-1} + s_\mathrm{c}) \tag{45}$$

and

$$\tilde{\chi}(x) = \chi(x\kappa^{-1} + s_\mathrm{c})/\chi(s_\mathrm{c}), \tag{46}$$

respectively. These functions are plotted for large values of L in figure 9, thus illustrating their expected collapse as L becomes large.
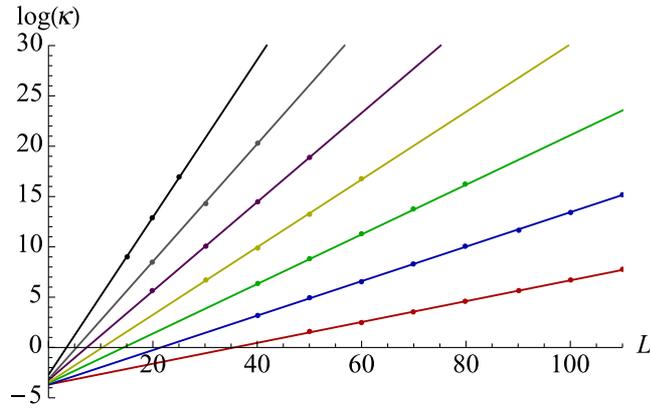
Figure 8. The logarithm of the scaling ratio κ defined in (43) as a function of L for $c = 0.2$ (red), $c = 0.3$ (blue), $c = 0.4$ (green), $c = 0.5$ (yellow), $c = 0.6$ (purple), $c = 0.7$ (gray) and $c = 0.8$ (black). Dots were obtained by solving the eigenvalue equation (8) numerically. Solid lines are linear fits.
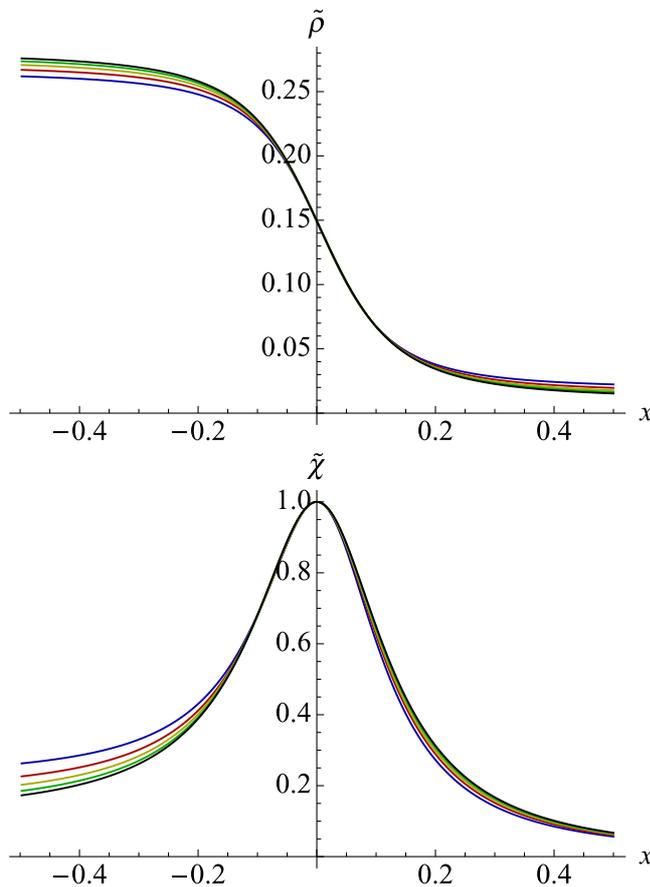
Figure 9. The scaling functions $\tilde{\rho}(x) = \rho(x\kappa^{-1} + s_{\mathrm{c}})$ (top) and $\tilde{\chi}(x) = \chi(x\kappa^{-1} + s_{\mathrm{c}})/\chi(s_{\mathrm{c}})$ (bottom) for $c = 0.3$ and for various L. The blue, red, green, yellow, and black lines correspond to $L = 60, 70, 80, 90$, and $L = 100$, respectively.

2.5. A variational formula in the infinite system size limit

In the previous section, we found numerically that the scaling functions are well defined with an exponential rescaling with the system size. Hereafter, we discuss how to derive those scaling properties analytically. With this purpose in mind, we consider the variational principle (10). We introduce a variational function $\tilde{\Phi}_{\mathrm{L}}(n)$ as

$$\tilde{\Phi}_{\mathrm{L}}(n) = \Phi^0(n) P_{\mathrm{eq}}(n)^{-1/2}. \tag{47}$$

By changing the variational parameter Φ^0 to $\tilde{\Phi}_{\mathrm{L}}$, we rewrite (10) as

$$L\psi(s) = \max_{\tilde{\Phi}_{\mathrm{L}} > 0} \sum_{n'} \widetilde{P}(n') \sum_n \tilde{\Phi}_{\mathrm{L}}(n) W_{n,n'} \tilde{\Phi}_{\mathrm{L}}(n')^{-1}, \tag{48}$$

where the distribution function $\widetilde{P}(n)$ is defined as

$$\widetilde{P}(n) = \frac{P_{\mathrm{eq}}(n) \tilde{\Phi}_{\mathrm{L}}(n)^2}{\sum_{\tilde{n}} P_{\mathrm{eq}}(\tilde{n}) \tilde{\Phi}_{\mathrm{L}}(\tilde{n})^2}. \tag{49}$$

We note that since, in (10), the optimal $\tilde{\Phi}_{\mathrm{L}}$ corresponds to the largest eigenvector Φ_{L}, the optimal distribution function $\widetilde{P}$ is equal to the modified equilibrium distribution function (15). Extensions of such variational principle are valid not only for equilibrium dynamics but also for non-equilibrium dynamics that violate the detailed balance condition. We refer the reader to reference [29] for details. In this section, before considering the finite-size scaling properties, we start by considering the $L \to \infty$ limit by assuming a large deviation principle in the optimal modified system holds.

Let us now introduce, similarly to (16), a variational function $\Delta \widetilde{F}$ as

$$\Delta \widetilde{F}(n) = -2 \log \tilde{\Phi}_{\mathrm{L}}(n), \tag{50}$$

and change the variational parameter $\tilde{\Phi}_{\mathrm{L}}$ to $\Delta \widetilde{F}$. We note that the optimal $\Delta \widetilde{F}$ is equal to the free energy difference ΔF_s defined in (16). The extremalization principle (48) can be rewritten as

$$\psi(s) = \frac{1}{L} \max_{\Delta \widetilde{F}} \sum_n \widetilde{P}(n) \left[\tilde{r}(n) - r(n) \right], \tag{51}$$

where $\tilde{r}(n)$ is defined as

$$\tilde{r}(n) = nc \left(1 - \frac{n}{L} \right) \mathrm{e}^{-\frac{1}{2}[\Delta \widetilde{F}(n+1) - \Delta \widetilde{F}(n)] - s} + n(1-c) \left(\frac{n}{L} - \frac{1}{L} \right) \mathrm{e}^{-\frac{1}{2}[\Delta \widetilde{F}(n-1) - \Delta \widetilde{F}(n)] - s}. \tag{52}$$

Now, we assume that the optimal modified distribution $\widetilde{P}$ scales, in the large L asymptotics, by following the large deviation form

$$\widetilde{P}(n) \sim \mathrm{e}^{-L\left[f_{\mathrm{e}}(n/L) + \tilde{f}(n/L) \right]}, \tag{53}$$

where $\tilde{f}(\rho)$ is an unknown function we determine below. This indicates that the variational function $\Delta \widetilde{F}(n)$ scales as $L\tilde{f}(\rho)$ with $\rho = n/L$, as $L \to \infty$. From these assumptions, (52) is rewritten as

$$\frac{\tilde{r}(L\rho)}{L} = \mathrm{e}^{-s} \left[\rho c (1-\rho) \mathrm{e}^{-\frac{1}{2}\tilde{f}'(\rho)} + \rho^2 (1-c) \mathrm{e}^{\frac{1}{2}\tilde{f}'(\rho)} \right] + O(1/L) \tag{54}$$

where $\tilde{f}'(\rho) = \frac{\partial \tilde{f}(\rho)}{\partial \rho}$. By substituting this into (51) and evaluating the summation within the saddle point approximation, we obtain, up to terms in $O(1/L)$

$$\psi(s) = \max_{\tilde{f} > 0} \frac{\int \mathrm{d}\rho \left\{ \mathrm{e}^{-s} \left[\rho c(1-\rho) \mathrm{e}^{-\frac{1}{2}\tilde{f}'(\rho)} + \rho^2(1-c) \mathrm{e}^{\frac{1}{2}\tilde{f}'(\rho)} \right] - r(L\rho)/L \right\} \mathrm{e}^{-L[f_e(\rho) + \tilde{f}(\rho)]}}{\int \mathrm{d}\rho \, \mathrm{e}^{-L[f_e(\rho) + \tilde{f}(\rho)]}} \tag{55}$$

Here $f_e(\rho)$ is the large deviation function (6). We now evaluate the integrals over ρ through the saddle point method. From (54), we read that the exponential dependence in L of the numerator and the denominator of (55) is the same. Assuming that the optimal function $f_e(\rho) + \tilde{f}(\rho)$ reaches its minimum at a unique point ρ^0, we have that the numerator and the denominator of (55) are both dominated by $\rho = \rho^0$. With the condition

$$\tilde{f}'(\rho^0) + f_e{}'(\rho^0) = 0, \tag{56}$$

this leads to the variational principle

$$\psi(s) = \max_{0 \leqslant \rho^0 \leqslant 1} \left\{ \mathrm{e}^{-s} \left[\rho^0 c(1-\rho^0) \mathrm{e}^{-\frac{1}{2}\tilde{f}'(\rho^0)} + (\rho^0)^2(1-c) \mathrm{e}^{\frac{1}{2}\tilde{f}'(\rho^0)} \right] - r(L\rho^0)/L \right\} \tag{57}$$

Finally, by substituting (56) into (57) and using the definition (6) of $f_e(\rho)$, we arrive at

$$\psi(s) = \max_{0 \leqslant \rho \leqslant 1} \left\{ 2\mathrm{e}^{-s} \sqrt{\rho^3(1-\rho)c(1-c)} - \left[\rho c(1-\rho) + (1-c)\rho^2 \right] \right\} + O(1/L) \tag{58}$$

Such variational formula describes the large-size behavior of large deviation of a wide class of stochastic models on the complete graph [8, 9, 24] or quantum annealing models [22]. In figure 1, the obtained $\lim_{L \to \infty} \psi(s)$, whose transitions occur at $s_c^\infty = 0$, is compared to finite-size results obtained by numerical diagonalization.

We now discuss how to extend the discussion presented in this subsection so as to obtain the finite-size scaling. A blunt perturbation in $1/L$ around (58) cannot be performed directly, since for instance it cannot describe how the $O(L^0)$ discontinuity of $K(s)$ at $s_c^\infty = 0$ is rounded at large but finite L. More generically, the free energy difference ΔF_s defined in (16), which allows one to recover $\psi(s)$, is exactly 0 at $s = 0$. One could thus expect that $\Delta F_s/L = O(1/L)$ at the transition point, using that $s_c = O(1/L)$ (section 2.2). However, because of the non-analyticity of $\Delta F_s/L$ with respect to s around the transition point s_c, one has in fact $\Delta F_s/L = O(1)$, as discussed in section 2.3. This explains the breakdown of a $1/L$ expansion of (58). In the next section, we propose a new method to overcome those difficulties without relying on a perturbative approach.

2.6. Analytical expressions for the scaling functions

Let us first consider the coexistence point $s = s_c$. We use the finite-size correction of the free energy obtained in section 2.3. We first define the finite-size free energy difference for each region as

$$f_i(\rho) = \Delta f_{s_c}(\rho) + \frac{1}{L} \Delta f_{s_c}^{(1)}(\rho) \tag{59}$$

for $\rho \leqslant \rho_\mathrm{c}^L$

$$f_\mathrm{a}(\rho) = \Delta f_{s_\mathrm{c}}(\rho) + \frac{1}{L}\Delta f_{s_\mathrm{c}}^{(1)}(\rho) \tag{60}$$

for $\rho > \rho_\mathrm{c}^L$. Then, the corresponding distribution function is

$$P^{s_\mathrm{c}}(n) = P_\mathrm{i}(n)\,1_{n \leqslant n_c^L} + P_\mathrm{a}(n)\,1_{n > n_c^L}, \tag{61}$$

where $P_\mathrm{i}(n)$ and $P_\mathrm{a}(n)$ are defined as

$$P_\mathrm{i}(n) = \frac{1}{Z_\mathrm{i} + Z_\mathrm{a}}P_\mathrm{eq}(n)\mathrm{e}^{-Lf_\mathrm{i}(n/L)} \tag{62}$$

$$P_\mathrm{a}(n) = \frac{1}{Z_\mathrm{i} + Z_\mathrm{a}}P_\mathrm{eq}(n)\mathrm{e}^{-Lf_\mathrm{a}(n/L)} \tag{63}$$

with the normalization constant

$$Z_\mathrm{i} = \sum_{n \leqslant n_\mathrm{c}} P_\mathrm{eq}(n)\mathrm{e}^{-Lf_\mathrm{i}(n/L)}, \tag{64}$$

$$Z_\mathrm{a} = \sum_{n > n_\mathrm{c}} P_\mathrm{eq}(n)\mathrm{e}^{-Lf_\mathrm{a}(n/L)}. \tag{65}$$

Here, we note $Z_\mathrm{i} = Z_\mathrm{a}$ from the definition (37) of ρ_c^L. In this system, there naturally arise two regions, $n \leqslant n_\mathrm{c}$ and $n > n_\mathrm{c}$, which represent the inactive phase and active phase, respectively. As seen below, this separation plays an important role in the exponentially fast scaling of section 2.4.

By using the result at $s = s_\mathrm{c}$, we consider the region around s_c ($s \sim s_\mathrm{c}$). Here, we propose an ansatz. That is, the distribution function around s_c is written as

$$P^s(n) = [1 + a^*(s)]\delta_{n \leqslant n_\mathrm{c}}P_\mathrm{i}(n) + [1 - a^*(s)]\delta_{n > n_\mathrm{c}}P_\mathrm{a}(n), \tag{66}$$

where $a^*(s)$ is a 'mixing function' to determine. This ansatz is inspired by the mathematically proven description of static and classical equilibrium first-order transitions in the coexistence region as described in [16,17] based on a Gibbs distribution picture. We should mention that in contrast to [16,17], our full distribution $P^s(n)$ does not describe a superposition between two elementary distributions, but a separation of the space of occupation number n into two regions presenting distributions of different nature. Also, we stress that the main difference between our method and their method appears in the mixing function $a^*(s)$, which is be determined by a variational principle as shown below. The dynamical thermodynamic formalism has a variational principle, which determines the stationary state, in contrast to the equilibrium thermodynamics. The mixing function $a^*(s)$ reflects this inevitable difference between these two thermodynamics.

To our knowledge, the ansatz (66) has not been used up to now in the dynamical approach we follow. In physical terms, the ansatz (66) allows us to handle the difficulty at the core of the extension of the infinite-size method presented in section 2.5. In the infinite-size limit, the variational maximum (48) is dominated by the most probable value of the occupation density ρ, yielding (58). In the finite-size limit this image however breaks

down in the vicinity of $s = s_\mathrm{c}$, where the active and inactive densities $\rho \simeq 0$ and $\rho \simeq c$ are in competition, and finer details than the mere maximum of the distribution of ρ have to be taken into account at large but finite L. The ansatz (66) describes the continuous transition, as s increases, from the active to the inactive *distribution* of density.

The distribution function (66) satisfies the normalization condition because $Z_\mathrm{i} = Z_\mathrm{a}$. From this expression and the relation (15), we obtain $\Phi_\mathrm{L}(n)$ (or the free energy difference $\Delta F_s(n)$) as

$$\Phi_\mathrm{L}(n) \propto \delta_{n \leqslant n_\mathrm{c}} \sqrt{1 + a^*(s)} \mathrm{e}^{-L f_\mathrm{i}(n/L)/2} + \delta_{n > n_\mathrm{c}} \sqrt{1 - a^*(s)} \mathrm{e}^{-L f_\mathrm{a}(n/L)/2}, \quad (67)$$

and the expectation values $\rho(s)$, $\chi(s)$ around s_c as

$$\rho(s) = \frac{\langle \rho \rangle_\mathrm{i}}{2} \left[1 + a^*(s)\right] + \frac{\langle \rho \rangle_\mathrm{a}}{2} \left[1 - a^*(s)\right], \quad (68)$$

$$\chi(s) = L \left\{ \frac{\langle \rho^2 \rangle_\mathrm{i}}{2} \left[1 + a^*(s)\right] + \frac{\langle \rho^2 \rangle_\mathrm{a}}{2} \left[1 - a^*(s)\right] - \rho(s)^2 \right\}, \quad (69)$$

where $\langle \ \rangle_\mathrm{i}$ and $\langle \ \rangle_\mathrm{a}$ are the expectation values in the active and the inactive phases defined as $\langle g \rangle_\mathrm{i} = 2 \sum_{n \leqslant n_\mathrm{c}} P_\mathrm{i}(n) g(n)$ and $\langle g \rangle_\mathrm{a} = 2 \sum_{n > n_\mathrm{c}} P_\mathrm{a}(n) g(n)$ respectively. When we know $a^*(s)$, we thus can calculate every scaling property around s_c.

For determining $a^*(s)$, we use the variational principle (51). We consider the variational function $\Psi(a)$ defined as

$$\Psi(a) = \frac{1}{L} \sum_n P^s(n) \left[\tilde{r}(n) - r(n)\right], \quad (70)$$

with

$$\tilde{r}(n) = nc \left(1 - \frac{n}{L}\right) \frac{\Phi_\mathrm{L}(n+1)}{\Phi_\mathrm{L}(n)} \mathrm{e}^{-s} + n(1-c) \left(\frac{n}{L} - \frac{1}{L}\right) \frac{\Phi_\mathrm{L}(n-1)}{\Phi_\mathrm{L}(n)} \mathrm{e}^{-s}, \quad (71)$$

where P^s and Φ_L in these expressions are (66) and (67) with the replacement of the mixing function $a^*(s)$ by a mixing parameter a. We determine $a^*(s)$ from the condition

$$\partial \Psi(a)/\partial a |_{a=a^*(s)} = 0. \quad (72)$$

For evaluating the variational function, we divide the region of the summation in (70) into three parts, (i) $n < n_\mathrm{c}$, (ii) $n > n_\mathrm{c} + 1$, and (iii) $n = n_\mathrm{c}$, $n_\mathrm{c} + 1$. For this, we define functions

$$\Psi_<(a) = (1/L) \sum_{n < n_\mathrm{c}} P^s(n) \left[\tilde{r}(n) - r(n)\right], \quad (73)$$

$$\Psi_>(a) = (1/L) \sum_{n > n_\mathrm{c}} P^s(n) \left[\tilde{r}(n) - r(n)\right], \quad (74)$$

$$\Psi_=(a) = (1/L) \sum_{n = n_\mathrm{c}, n_\mathrm{c} + 1} P^s(n) \left[\tilde{r}(n) - r(n)\right]. \quad (75)$$

For (i) and (ii), one can easily find that the dependence in the mixing parameter a is linear because $\tilde{r}(n)$ is an independent function of a. Indeed, we obtain

$$\Psi_<(a) = (1+a)\Omega_<, \tag{76}$$

$$\Psi_>(a) = (1-a)\Omega_>, \tag{77}$$

where $\Omega_<$ and $\Omega_>$ are constants defined as

$$\Omega_< = \frac{1}{2L}\left\langle \tilde{r}_i e^{-s} - r \right\rangle_i, \tag{78}$$

$$\Omega_> = \frac{1}{2L}\left\langle \tilde{r}_a e^{-s} - r \right\rangle_a, \tag{79}$$

with the definition of $\tilde{r}_{i,a}(n)$ as

$$\tilde{r}_{i,a}(n) = nc\left(1 - \frac{n}{L}\right)\frac{e^{-Lf_{i,a}((n+1)/L)/2}}{e^{-Lf_{i,a}(n/L)/2}} + n(1-c)\left(\frac{n}{L} - \frac{1}{L}\right)\frac{e^{-Lf_{i,a}((n-1)/L)/2}}{e^{-Lf_{i,a}(n/L)/2}}. \tag{80}$$

Different from these parts, however, $\Psi_=(a)$ does not depend linearly on the mixing parameter a. Because of this fact, we have to consider this part in spite of it being exponentially small compared with $\Psi_>(a)$ and $\Psi_<(a)$. $\Psi_=(a)$ is

$$\Psi_=(a) = \frac{n_c}{L}c(1 - \frac{n_c}{L})\frac{\Phi_L(n_c+1)}{\Phi_L(n_c)}P^s(n_c)e^{-s}$$
$$+ \frac{(n_c+1)}{L}(1-c)\frac{n_c}{L}\frac{\Phi_L(n_c)}{\Phi_L(n_c+1)}P^s(n_c+1)e^{-s} + \cdots, \tag{81}$$

where $\cdots$ stands for the terms that are proportional to a. The nonlinear dependence in the mixing parameter a is crucial (without it, the variational principle (72) would be of no use) and arises from the finite-size correction to the free energy difference obtained at the end of section 2.3.

By using $P^s(n+1)\Phi_L(n)/\Phi_L(n+1) = P^s(n)\Phi_L(n+1)P_{eq}(n+1)/(\Phi_L(n)P_{eq}(n))$, we find that the first term and the second term in the right-hand side of (81) are equal. We thus have

$$\Psi_=(a) = 2\sqrt{1-a^2}\frac{n_c}{L}c(1 - \frac{n_c}{L})P_i(n_c)\frac{e^{-Lf_a((n_c+1)/L)/2}}{e^{-Lf_i(n_c/L)/2}}e^{-s} + \cdots. \tag{82}$$

By defining constants

$$\Omega_= = 2\frac{n_c}{L}c(1 - \frac{n_c}{L})P_i(n_c)\frac{e^{-Lf_a((n_c+1)/L)/2}}{e^{-Lf_i(n_c/L)/2}}e^{-s}, \tag{83}$$

we obtain an expression of $\Psi(a)$ that represents the a dependence. That is,

$$\Psi(a) = \Omega_< + \Omega_> + a(\Omega_< - \Omega_>) + \sqrt{1-a^2}\Omega_=. \tag{84}$$

Thus, by maximizing $\Psi(a)$ with respect to a, we arrive at the expression of $a^*(s)$ as

$$a^*(s) = \frac{A}{\sqrt{1+A^2}}, \tag{85}$$

where A is

$$A = (\Omega_< - \Omega_>)/\Omega_=. \tag{86}$$

Now, by using (85) and (86), we discuss the scaling properties. First, we focus on the scaling ratio κ defined in (43). We know that $a^*(s_c) = 0$ by definition. From (78), (79), (85) and (86), we thus obtain an equation for s_c as

$$\frac{1}{L} \left\langle \tilde{r}_i e^{-s_c} - r \right\rangle_i = \frac{1}{L} \left\langle \tilde{r}_a e^{-s_c} - r \right\rangle_a. \tag{87}$$

Then, we expand A around $s = s_c$ by using this condition. By denoting $\Omega_=|_{s=s_c}$ by $\Omega_=^c$, we obtain

$$A = -\frac{s - s_c}{\Omega_=^c} \left[\left\langle \frac{r}{2L} \right\rangle_i - \left\langle \frac{r}{2L} \right\rangle_a \right] + O((s - s_c)^2), \tag{88}$$

from which, with (68) and (85), we find the scaling ratio $\kappa = -\partial \rho(s)/\partial s|_{s=s_c}$ as

$$\kappa = \frac{1}{\Omega_=^c} \left[\left\langle \frac{\rho}{2} \right\rangle_i - \left\langle \frac{\rho}{2} \right\rangle_a \right] \left[\left\langle \frac{r}{2L} \right\rangle_i - \left\langle \frac{r}{2L} \right\rangle_a \right]. \tag{89}$$

Here, we note that the L dependence in κ mainly comes from $P_i(n_c)$ in $\Omega_=^c$ because each of the other terms converges to each corresponding value in the $L \to \infty$ limit. That is, when L is large, $\log \kappa \to -\log P_i(n_c) + \text{const}$. By using the large deviation property of $P_i(n_c)$, we thus arrive at

$$\frac{1}{L} \log \kappa \longrightarrow f_{s_c}(\rho_c^\infty) = -\frac{1}{2} \log(1 - c) \qquad \text{as} \quad L \to \infty. \tag{90}$$

We note that the slope of the straight lines in figure 8 is the height of the large deviation function from bottom to the connecting point ($\rho = \rho_c^\infty$). This reminds us of the instantonic approach used in [21]. Along a similar vein, Bapst and Semerjian derived a formula determining the exponentially small gap in the quantum ferromagnet [22]. In the next section, by using our approach, we will re-derive this formula.

Next, we obtain the expression of the scaling function. By combining the definition of x in (44) with (88) and (89), we know

$$A = \frac{2x}{\langle \rho \rangle_a - \langle \rho \rangle_i} + O(\kappa^{-1}). \tag{91}$$

From this with (68), (69) and (85), we find the analytical expression of $\tilde{\rho}(x)$ and $\tilde{\chi}(x)$ as

$$\tilde{\rho}(x) = \frac{1}{2} \left[\langle \rho \rangle_i + \langle \rho \rangle_a - \frac{2x}{\sqrt{1 + 4x^2 \left[\langle \rho \rangle_i - \langle \rho \rangle_a \right]^{-2}}} \right], \tag{92}$$

$$\tilde{\chi}(x) = \frac{1}{\langle \rho^2 \rangle_i + \langle \rho^2 \rangle_a - \left[\langle \rho \rangle_i + \langle \rho \rangle_a \right]^2 / 2}$$
$$\times \left[\langle \rho^2 \rangle_i + \langle \rho^2 \rangle_a - \frac{2x \left[\langle \rho^2 \rangle_i - \langle \rho^2 \rangle_a \right] \left[\langle \rho \rangle_i - \langle \rho \rangle_a \right]^{-1}}{\sqrt{1 + 4x^2 \left[\langle \rho \rangle_i - \langle \rho \rangle_a \right]^{-2}}} - 2\tilde{\rho}(x)^2 \right], \tag{93}$$
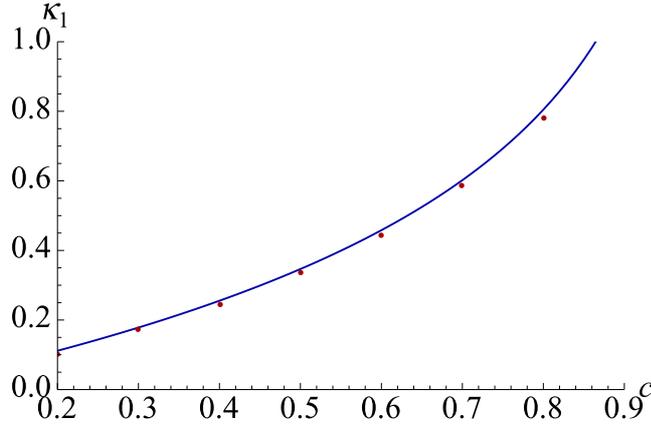
Figure 10. κ_1 (the exponent in the exponential behavior of $\kappa \sim e^{\kappa_1 L}$). We estimated κ_1 for $c = 0.2, 0.3, \ldots, 0.8$ from figure 8 for finite L and plot those as the red dots. Also, we draw the analytical result $-\frac{1}{2}\log(1-c)$ (blue line) expected in the infinite L limit, see (90). The small discrepancy corresponds to finite-size effects, see (96).

where we omit the exponentially small deviation $O(\kappa^{-1})$. The only parameters appearing in these expressions are the expectation value and the variance of ρ in each of the active and inactive phases. They can still bear a finite-size dependency, which is important for numerical analysis at large but finite L, as illustrated in figure 11. Because these parameters converge in the $L \to \infty$ limit, each of the expressions (92) and (93) also converge to a limit function. Indeed, from the modified free energy (33) and (34), we obtain $\lim_{L\to\infty} \langle \rho \rangle_{\mathrm{i}} = 0$ and $\lim_{L\to\infty} \langle \rho \rangle_{\mathrm{a}} = c$. This leads to the following infinite-size scaling functions:

$$\tilde{\rho}_\infty(x) = \lim_{L\to\infty} \tilde{\rho}(x) = \frac{1}{2}\left[c - \frac{2x}{\sqrt{1 + 4x^2 c^{-2}}} \right], \tag{94}$$

$$\tilde{\chi}_\infty(x) = \lim_{L\to\infty} \tilde{\chi}(x) = \frac{c^2}{c^2 + 4x^2}. \tag{95}$$

We stress that for the derivation of (90), (92) and (93), we haven't used the details of this system, e.g. $r(n)$, $f_{\mathrm{i}}(\rho)$, $f_{\mathrm{a}}(\rho)$. It indicates that the scaling results (90), (92) and (93) should also hold in other systems. We will see an example of such an extension to other systems in part section 3, for a mean-field quantum ferromagnet.

Finally, we numerically check the obtained results (90), (92), and (93). From figure 8, we estimate the slopes of the straight lines of $\log \kappa$. We denote it by κ_1. We plot κ_1 for $c = 0.2, 0.3, \ldots, 0.8$ in figure 10 (red dots) and at the same time we also draw $(-1/2)\log(1-c)$ as a function of c (blue line), which is (90). We can see how they coincide. Next, in figure 11, we plot the analytical expressions (92), (93) and the corresponding numerical results, as blue dotted lines and red solid lines, respectively.

The accuracy of the coincidence between the numerical and the analytical results is amazing. On the same figure, we also plot the infinite-size scaling functions (94) and (95) in yellow lines. One can see the deviation between the infinite ones and the finite ones. This indicates that larger system sizes are required to observe the convergence to the infinite-size scaling functions. It is worth mentioning that even for the relatively small
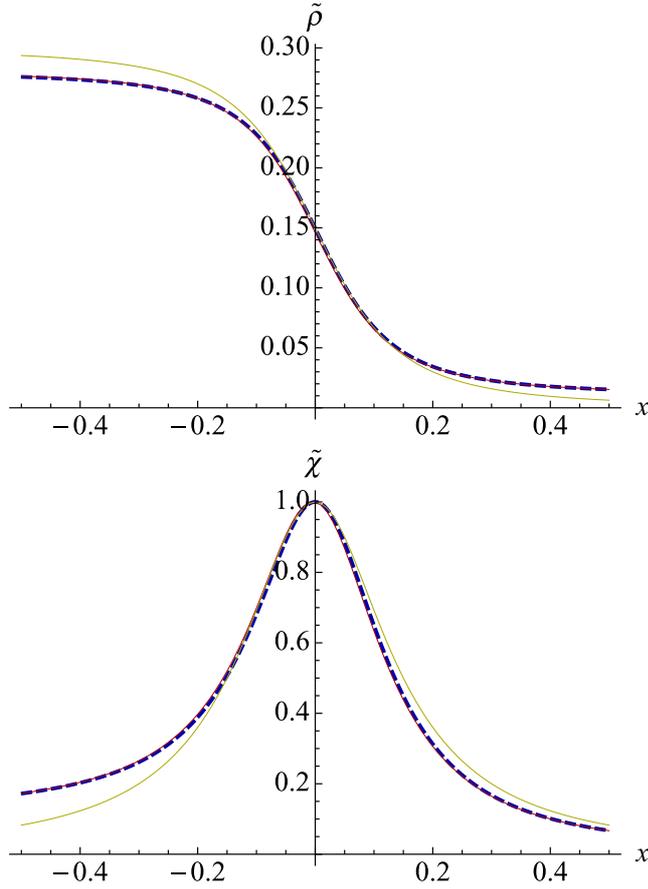
Figure 11. Analytical results for the scaling functions $\tilde{\rho}(x) = \rho(x\kappa^{-1} + s_c)$ (up) and $\chi(x) = \chi(x\kappa^{-1} + s_c)/\chi(s_c)$ (down) for $c = 0.3$ for $L = 100$. The solid red lines are the analytical results (92) and (93). The dashed blue lines are the numerical results, which are the same as in figure 9. We also plot the infinite-size scaling functions (94) and (95) as the yellow lines, which illustrate the importance of large but finite-size contributions.

system sizes, the finite-size scaling formulæ (92) and (93) show good agreement with the numerical lines. Because the numerical diagonalization becomes harder as the system size becomes larger, the finite-size scaling functions (92) and (93) make checking the validity of our formulation easier. Furthermore, we also evaluate s_c by using (87). The result is

$$s_c = 1/(2Lc(1-c)) + O(1/L^2), \qquad (96)$$

which is checked numerically in figure 1. See appendix A for the details of the evaluation. This tells us that the upper bound in (24) is actually saturated.

2.7. Scaling function of $\partial\psi(s)/\partial s$

So far, we have focused on the scaling property of $\rho(s)$ and $\chi(s)$. In a similar vein, in this section, we will show the scaling function of $\partial\psi(s)/\partial s$ and $\partial^2\psi(s)/\partial s^2$, which correspond to the expectation value and the susceptibility of the activity in the modified system.

First, the expectation value of the activity in the modified system can be calculated as

$$-\frac{\partial\psi(s)}{\partial s} = \sum_n \sum_{n'} P^s(n)w(n \to n') = \sum_n P^s(n)r(n), \qquad (97)$$

where $r(n)$ is the escape rate given as (3). Since only n and n^2 terms constitute $r(n)$, the expectation value of $\partial\psi(s)/\partial s$ can be expressed by using only $\rho(s)$ and $\chi(s)$. Indeed, with relations $\rho(s)L = \langle n \rangle^s_{\text{eq}}$ and $\langle n^2 \rangle^s_{\text{eq}} = L\chi(s) + L^2\rho(s)^2$, we obtain

$$-\frac{\partial\psi(s)}{\partial s} = \rho(s)(Lc + c - 1) + \rho(s)^2 L(1 - 2c) + (1 - 2c)\chi(s). \qquad (98)$$

By substituting these $\rho(s)$ and $\chi(s)$ by (68) and (69), changing the variables to x, and using (85) and (91), we rewrite it as

$$-\frac{\partial\psi(s)}{\partial s}\Big|_{s=s_c+\kappa^{-1}x} = \frac{1}{2}\left[\langle\rho\rangle_i + \langle\rho\rangle_a\right](Lc + c - 1) + \frac{1-2c}{2}L\left[\langle\rho^2\rangle_i + \langle\rho^2\rangle_a\right] \qquad (99)$$

$$+\frac{2x\left[\langle\rho_a\rangle - \langle\rho\rangle_i\right]^{-1}}{\sqrt{1 + 4x^2\left[\langle\rho_a\rangle - \langle\rho\rangle_i\right]^{-2}}}$$

$$\times\left\{\frac{1}{2}\left[\langle\rho\rangle_i - \langle\rho\rangle_a\right](Lc + c - 1) + \frac{1-2c}{2}L\left[\langle\rho^2\rangle_i - \langle\rho^2\rangle_a\right].\right\} \qquad (100)$$

Finally, from this expression, we arrive at the asymptotic expression of $\partial\psi(s)/\partial s$ and $\partial^2\psi(s)/\partial s^2$ as

$$-\lim_{L\to\infty}\frac{1}{L}\frac{\partial\psi(s)}{\partial s}\Big|_{s=s_c+\kappa^{-1}x} = c^2(1 - c)\left[1 - \frac{2xc^{-1}}{\sqrt{1 + 4x^2c^{-2}}}\right], \qquad (101)$$

$$\lim_{L\to\infty}\frac{1}{L\kappa}\frac{\partial^2\psi(s)}{\partial s^2}\Big|_{s=s_c+\kappa^{-1}x} = 2c(1 - c)\frac{1}{(1 + 4x^2c^{-2})^{3/2}}. \qquad (102)$$

The results of this subsection are directly related to the ones from (94) and (95) on the density and variance of occupied sites, and we believe that this connection is generic. The forms (101) and (102) provide us with a complete description of the fluctuations of the dynamical activity around the transition point, where the fluctuations of the activity are at the origin of the transition itself.

3. Mean-field quantum ferromagnet and the scaling function

In this section, we apply the method in the previous section to a mean-field quantum ferromagnet. We will show that this system has the same scaling functions as (92) and (93). Furthermore, by applying our method to this model, we re-derive a formula that gives the exponent of an exponentially small gap at the quantum phase transition point [22].

3.1. Set up

Let us consider L interacting $1/2$ spins. The Hilbert space is spanned by the space $\{|\vec{\sigma}\rangle \mid \vec{\sigma} = (\sigma_1, \cdots, \sigma_L) \in \{-1, +1\}^N\}$. We denote the Pauli matrices acting on the i-th spin by $\hat{\sigma}_i^x$, $\hat{\sigma}_i^y$, and $\hat{\sigma}_i^z$. These matrices satisfy $\sigma_i^z|\vec{\sigma}\rangle = \sigma_i|\vec{\sigma}\rangle$, $\sigma_i^x|\vec{\sigma}\rangle = |\vec{\sigma}^{(i)}\rangle$, where $\vec{\sigma}^{(i)}$ is the configuration in which the i-th spin is flipped. The transverse and the longitudinal magnetizations are defined as

$$\hat{m}^x = \frac{1}{L}\sum_{i=1}^{L}\hat{\sigma}_i^x, \tag{103}$$

$$\hat{m}^z = \frac{1}{L}\sum_{i=1}^{L}\hat{\sigma}_i^z. \tag{104}$$

The Hamiltonian of the mean-field p-spin ferromagnet is defined as

$$\hat{H} = -L(\hat{m}^z)^p - \Gamma L\hat{m}^x \tag{105}$$

There is a phase transition in this model for a special value of Γ. It is known that for the $p = 2$ (quantum Curie–Weiss model) the transition is second-order, whereas for the $p \geqslant 3$ the transition is first-order. See reference [22] for the details of the thermodynamic properties of this model.

Here, we discuss the eigenvalues of the Hamiltonian $\hat{H}$. We denote by $|\Phi\rangle$ the eigenstate, and by E the eigenvalue. We especially focus on the eigenstates, where the interchanges of two spins are permitted. In other words, we focus on the eigenstates that only depend on $m^z = (1/L)\sum_{i=1}^{L}\sigma_i^z$:

$$\langle\vec{\sigma}|\Phi\rangle = \Phi(m^z). \tag{106}$$

We note that the ground state of $\hat{H}$ lies in this symmetric subspace. See reference [22] for the proof. By multiplying the eigenvalue equation $\hat{H}|\Phi\rangle = E|\Phi\rangle$ by $\langle\vec{\sigma}|$ from the left, and using (106), we obtain

$$-L(m^z)^p\Phi(m^z) - \Gamma L\frac{1}{L}\sum_{i=1}^{L}\left[\frac{1+\sigma_i^z}{2}\Phi(m^z - 2/L) + \frac{1-\sigma_i^z}{2}\Phi(m^z + 2/L)\right] = E\Phi(m^z), \tag{107}$$

which leads to an eigenvalue equation for the symmetric space,

$$\sum_{m'\in\mathcal{M}}H_{m,m'}\Phi(m') = \frac{E}{L}\Phi(m), \tag{108}$$

where $\mathcal{M} = \{-1, -1 + 2/L, \cdots, 1 - 2/L, 1\}$ and

$$H_{m,m'} = -(m)^p\delta_{m,m'} - \Gamma\left[\frac{1+m}{2}\delta_{m-2/L,m'} + \frac{1-m}{2}\delta_{m+2/L,m'}\right]. \tag{109}$$

Thanks to the symmetry of the eigenstate, the dimension of the eigenvalue problem is reduced to $L + 1$. We note that the matrix $H_{m,m'}$ is not symmetric although the Hamiltonian $\hat{H}$ is Hermitian. Here, we define the number of the state $p(m)$ by

$$p(m) \equiv \sum_{\vec{\sigma}} \delta_{m^z(\vec{\sigma}),m} = \frac{L!}{((1+m)L/2)!((1-m)L/2)!} \frac{1}{2^L}. \tag{110}$$

With this function, we may calculate the expectation value of a function $g(\hat{m}^z)$ in these symmetric eigenstates from

$$\frac{\langle \Phi | g(\hat{m}^z) | \Phi \rangle}{\langle \Phi | \Phi \rangle} = \sum_m g(m) p^\Gamma(m), \tag{111}$$

where the distribution function $p^\Gamma(m)$ is defined as

$$p^\Gamma(m) = \frac{p(m)|\Phi(m)|^2}{\sum_m p(m)|\Phi(m)|^2}. \tag{112}$$

Hereafter, we focus on the ground state of the system. The expectation value and the variance of $\hat{m}^z$ for the ground state is also denoted by $m(\Gamma)$ and $\sigma(\Gamma)$, which are calculated as

$$m(\Gamma) = \sum_m m p^\Gamma(m), \tag{113}$$

and

$$\sigma(\Gamma) = L \sum_m (m - m(\Gamma))^2 p^\Gamma(m). \tag{114}$$

The ground state is determined by a variational principle. That is, the ground state energy E satisfies

$$E = \min_{|\Psi\rangle} \frac{\langle \Psi | \hat{H} | \Psi \rangle}{\langle \Psi | \Psi \rangle}, \tag{115}$$

where the optimum is reached at the ground state $|\Phi\rangle$. Because the ground state is in the symmetric space [22], we know that $|\Phi\rangle$ satisfies (106). This allows us to rewrite (115) as

$$\frac{E}{L} = \min_{\tilde{\Phi} > 0} \sum_m \tilde{p}(m) \sum_{m'} \tilde{\Phi}(m)^{-1} H_{m,m'} \tilde{\Phi}(m'), \tag{116}$$

where $\tilde{p}(m)$ is defined as

$$\tilde{p}(m) = \frac{p(m)\tilde{\Phi}(m)^2}{\sum_m p(m)\tilde{\Phi}(m)^2}. \tag{117}$$

The optimal $\tilde{p}$ is equal to the ground state distribution function p^Γ. The variational principle has the same structure as (48). The modified distribution for the FA model (49) (or) (15) corresponds to the ground state of the quantum system (117) (or) (112). This correspondence indicates that we might use the same technique as previously to approach the finite-size properties for the quantum system—which we indeed implement in the following subsections.

3.2. Results in infinite-size limit

By assuming the large deviation property for the ground state, we first show a variational principle for the ground state energy in $L \to \infty$ and determine the magnetization and the transverse field corresponding to the first-order phase transition.

In the variational principle (48), we assume a large deviation principle for $\tilde{p}(m)$: $\tilde{p}(m) \sim \mathrm{e}^{-L\tilde{f}(m)}$ with a large deviation function $\tilde{f}(m)$. This indicates that $\tilde{\Phi}(m)$ also satisfies $\tilde{\Phi} \sim \mathrm{e}^{-L\tilde{\phi}(m)/2}$ with a large deviation function $\tilde{\phi}(m)$. From the large deviation property of $p(m)$, we have the relationship between $\tilde{f}(m)$ and $\tilde{\phi}(m)$ as

$$\tilde{f}(m) = \tilde{\phi}(m) + \frac{1+m}{2}\log(1+m) + \frac{1-m}{2}\log(1-m). \tag{118}$$

The saddle point equation for m is $\partial \tilde{f}(m)/\partial m = 0$, which leads to

$$\frac{\partial \tilde{\phi}(m)}{\partial m} = \frac{1}{2}\log\frac{1+m}{1-m}. \tag{119}$$

By evaluating the variational principle (48) with the saddle point approximation, and using (119) in it, we obtain

$$\frac{E}{L} = \min_m \left[-m^p - \Gamma\sqrt{1-m^2} \right]. \tag{120}$$

This variational formula is well known. See [22], for example. By solving this variational formula, we obtain an equation determining the expectation value of the magnetization m^*, which is

$$m^*\Gamma = p\,(m^*)^{p-1}\sqrt{1-(m^*)^2}. \tag{121}$$

For $p \geqslant 3$, the system has the first-order phase transition [22] with a special value of Γ, which we denote Γ_c^∞. At the transition point, there are two solutions to the variational problem (120), corresponding to the paramagnetic solution $m_\infty^{\mathrm{pa}} = 0$ and the ferromagnetic solution m_∞^{fe}. Γ_c^∞ and m_∞^{fe} are determined from the conditions

$$\left[-m^p - \Gamma_c^\infty\sqrt{1-m^2} \right]\Big|_{m_\infty^{\mathrm{pa}}=0} = \left[-m^p - \Gamma_c^\infty\sqrt{1-m^2} \right]\Big|_{m=m_\infty^{\mathrm{fe}}} \tag{122}$$

and (121) with the replacement of Γ and m^* by Γ_c^∞ and m_∞^{fe}.

In figure 12, we plot numerical examples of E/L and of the corresponding optimal m for $p = 3$ obtained from the variational principle (120). At the same time, we also plot the numerical examples of E/L, $m(\Gamma)$, and $\sigma(\Gamma)$ obtained from the direct diagonalization of the matrix (109) for finite-size systems. We can see the first-order phase transition around $\Gamma_c^\infty \simeq 1.3$ in the figure. Also, we can see the finite-size correction of magnetization and susceptibility, which is the next target we consider.

3.3. Finite-size structure—scaling functions

Now, we ask how to determine the finite-size structure shown in figure 12. For this purpose, we introduce the transition point Γ_c^L for the finite-size system as

$$\Gamma_c^L = \mathrm{Argmax}_\Gamma \sigma(\Gamma), \tag{123}$$
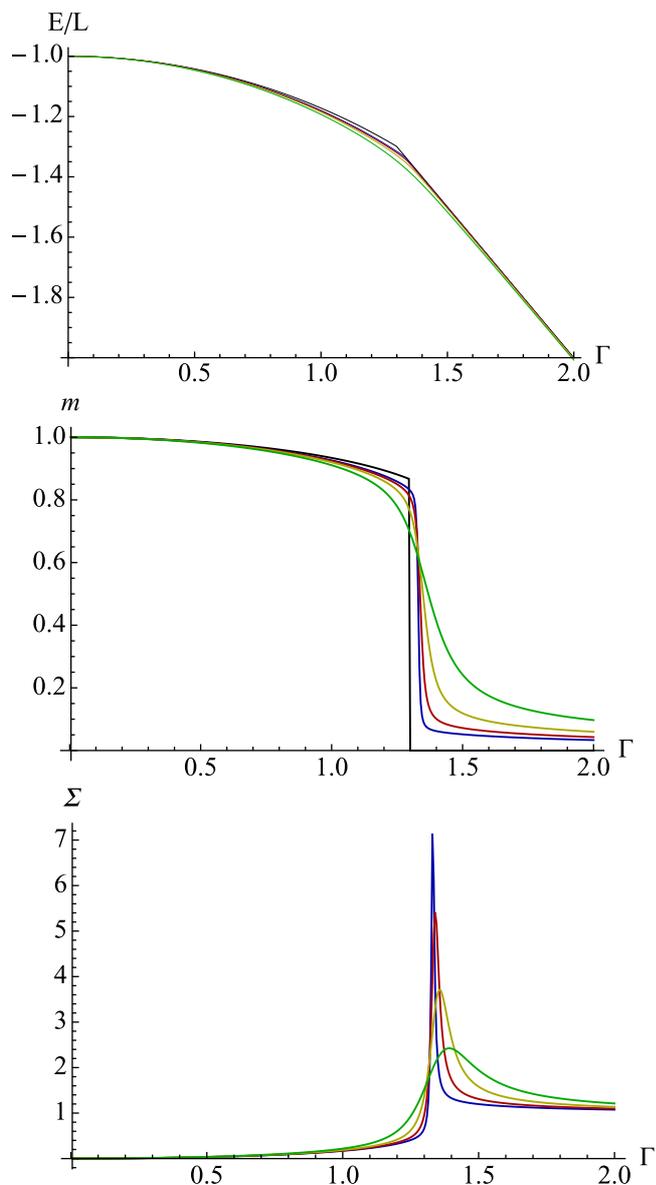
Figure 12. The ground state energy E/L (the black line on the upper figure) and the corresponding m^* (the black line on the center figure) in the variational principle (120). At the same time, we also plot E/L (upper), $m(\Gamma)$ (center) and $\sigma(\Gamma)$ (lower) obtained by the numerical diagonalization of the matrix (109). Blue, red, yellow and green lines correspond to $L = 50, 40, 30$, and 20, respectively.

which depends on L. Then we define the scaling ratio κ by $-\partial m(\Gamma_{\rm c}^L)/\partial \Gamma$. By using these quantities, we define scaling functions

$$\tilde{m}(x) = m(\Gamma_{\rm c}^L + x\kappa^{-1}), \tag{124}$$

and

$$\tilde{\sigma}(x) = \frac{\sigma(\Gamma_{\rm c}^L + x\kappa^{-1})}{\sigma(\Gamma_{\rm c}^L)}. \tag{125}$$

The question is how we determine the analytical expression of those scaling functions. For this, we apply the same method as the previous section for the KCM. First, we consider the distribution function $p^\Gamma(m)$ at the transition point. We assume that the distribution function is divided into two regions, the paramagnetic region $P_{\rm p}(m)$ and the ferromagnetic region $P_{\rm f}(m)$:

$$p^{\Gamma_{\rm c}^L}(m) = \delta_{m \leqslant m_{\rm c}} P_{\rm p}(m) + \delta_{m > m_{\rm c}} P_{\rm f}(m), \tag{126}$$

where $m_{\rm c}$ is the boundary of these two regions, which may be defined as the valley between two peaks for $\log P_{\rm p}(m)$. We note that $P_{\rm p}(m)$ and $P_{\rm f}(m)$ satisfy the condition of first-order phase transitions

$$\sum_{m \leqslant m_{\rm c}} P_{\rm p}(m) = \sum_{m > m_{\rm c}} P_{\rm f}(m) = 1/2. \tag{127}$$

Next, for the region around $\Gamma_{\rm c}^L$, we assume that p^Γ is written as

$$p^\Gamma(m) = (1 + a^*(\Gamma)) \delta_{m \leqslant m_{\rm c}} P_{\rm p}(m) + (1 - a^*(\Gamma)) \delta_{m > m_{\rm c}} P_{\rm f}(m), \tag{128}$$

where $a^*(\Gamma)$ is a mixing function of Γ. We note that the normalization condition is satisfied due to (127). From the distribution function, we can calculate $m(\Gamma)$, $\sigma(\Gamma)$ as

$$m(\Gamma) = \frac{\langle m \rangle_{\rm p}}{2} \left[1 + a^*(\Gamma) \right] + \frac{\langle m \rangle_{\rm f}}{2} \left[1 - a^*(\Gamma) \right], \tag{129}$$

$$\sigma(\Gamma) = L \left\{ \frac{\langle m^2 \rangle_{\rm p}}{2} \left[1 + a^*(\Gamma) \right] + \frac{\langle m^2 \rangle_{\rm f}}{2} \left[1 - a^*(\Gamma) \right] - m(\Gamma)^2 \right\}, \tag{130}$$

where $\langle \ \rangle_{\rm p}$ and $\langle \ \rangle_{\rm f}$ are the expectation values in the paramagnetic phase and the ferromagnetic phase, respectively, which are defined as $\langle g \rangle_{\rm p} = 2 \sum_{m \leqslant m_{\rm c}} P_{\rm p}(m) g(m)$ and $\langle g \rangle_{\rm f} = 2 \sum_{m > m_{\rm c}} P_{\rm f}(m) g(m)$. For the determination of $a^*(\Gamma)$, we use the variational principle (116). Indeed, from (128) with (112), we have $\Phi(m)$. By substituting the obtained $\Phi(m)|_{a^*(\Gamma)=a}$ and $p^\Gamma(m)|_{a^*(\Gamma)=a}$ into the variational functional of (116) and maximizing it with respect to a, we obtain the optimal a^*, which corresponds to $a^*(\Gamma)$. The result is

$$a^*(\Gamma) = \frac{x \left[\langle m \rangle_{\rm p} - \langle m \rangle_{\rm f} \right]^{-1}}{\sqrt{1 + 4x^2 \left[\langle m \rangle_{\rm p} - \langle m \rangle_{\rm f} \right]^{-2}}} + O(\kappa^{-1}). \tag{131}$$

with $x = \kappa(\Gamma - \Gamma_{\rm c})$. Combining it with (129) and (130), we obtain

$$\tilde{m}(x) = \frac{1}{2} \left[\langle m \rangle_{\rm p} + \langle m \rangle_{\rm f} - \frac{2x}{\sqrt{1 + 4x^2 \left[\langle m \rangle_{\rm p} - \langle m \rangle_{\rm f} \right]^{-2}}} \right], \tag{132}$$

$$\tilde{\sigma}(x) = \frac{1}{C} \left[\langle m^2 \rangle_{\rm p} + \langle m^2 \rangle_{\rm f} - \frac{2x \left[\langle m^2 \rangle_{\rm p} - \langle m^2 \rangle_{\rm f} \right] \left[\langle m \rangle_{\rm p} - \langle m \rangle_{\rm f} \right]^{-1}}{\sqrt{1 + 4x^2 \left[\langle m \rangle_{\rm p} - \langle m \rangle_{\rm f} \right]^{-2}}} - 2\tilde{m}(x)^2 \right], \tag{133}$$

where C is

$$C = \left\langle m^2 \right\rangle_{\mathrm{p}} + \left\langle m^2 \right\rangle_{\mathrm{f}} - 2\tilde{m}(0)^2. \tag{134}$$

These expressions are equivalent to the relations (92) and (93) that we obtained in our study of the KCM. Noticing that $\lim_{L\to\infty} \left\langle m \right\rangle_{\mathrm{p}} = \lim_{L\to\infty} \left\langle m^2 \right\rangle_{\mathrm{p}} = 0$, $\lim_{L\to\infty} \left\langle m \right\rangle_{\mathrm{f}} = m_\infty^{\mathrm{fe}}$, and $\lim_{L\to\infty} \left\langle m^2 \right\rangle_{\mathrm{f}} = (m_\infty^{\mathrm{fe}})^2$, we also obtain the infinite-size scaling functions:

$$\tilde{m}_\infty(x) = \lim_{L\to\infty} \tilde{m}(x) = \frac{1}{2}\left[m_\infty^{\mathrm{fe}} - \frac{2x}{\sqrt{1 + 4x^2(m_\infty^{\mathrm{fe}})^{-2}}} \right], \tag{135}$$

$$\tilde{\sigma}_\infty(x) = \lim_{L\to\infty} \tilde{\sigma}(x) = \frac{(m_\infty^{\mathrm{fe}})^2}{(m_\infty^{\mathrm{fe}})^2 + 4x^2}, \tag{136}$$

which correspond to (94) and (95). We check the obtained results in figure 13, from which one can see that (132) and (133) (solid red lines) show good agreement with the numerical results from direct diagonalization (blue dashed lines). As the same as the previous section, we also note that large system sizes are required to observe the convergence to the infinite-size scaling functions (135) and (136).

3.4. Finite-size structure—scaling factor and exponentially small gap

Finally, we derive the exponent of the scaling factor κ, which is equivalent to the exponentially small gap derived in [22].

We first define the free energy for the ground state at the transition point $\Gamma_{\mathrm{c}}^\infty$ by

$$f_{\Gamma_{\mathrm{c}}^\infty}(m) = -\lim_{L\to\infty} \frac{1}{L} \log p^{\Gamma_{\mathrm{c}}^\infty}(m). \tag{137}$$

Then, using the same argument as for (90), we obtain the exponent κ

$$\lim_{L\to\infty} \frac{1}{L} \log \kappa = f_{\Gamma_{\mathrm{c}}^\infty}(m_{\mathrm{c}}^\infty), \tag{138}$$

where $m_{\mathrm{c}}^\infty = \lim_{L\to\infty} m_{\mathrm{c}}$ represents the connecting point between the paramagnetic and the ferromagnetic regions in the infinite system size limit.

Next, we determine the free energy. We start from the ground state of the eigenvalue equation for $\Gamma = \Gamma_{\mathrm{c}}^\infty$,

$$-m^p - \Gamma_{\mathrm{c}}^\infty \left[\frac{1+m}{2}\frac{\Phi(m - 2/L)}{\Phi(m)} + \frac{1-m}{2}\frac{\Phi(m + 2/L)}{\Phi(m)} \right] = \frac{E}{L}, \tag{139}$$

which is obtained from (108). Now, we assume a large deviation principle. That is, we set $\Phi(m) = \mathrm{e}^{-(L/2)\phi(m)}$ in (139). The leading term of (139) is

$$-m^p - \Gamma_{\mathrm{c}}^\infty \left[\frac{1+m}{2}\mathrm{e}^{\partial\phi/\partial m} + \frac{1-m}{2}\mathrm{e}^{-\partial\phi/\partial m} \right] = e_{\mathrm{c}}^\infty, \tag{140}$$

where we define $\lim_{L\to\infty} E/L|_{\Gamma=\Gamma_{\mathrm{c}}^\infty} \equiv e_{\mathrm{c}}^\infty$. By solving this equation, we obtain two solutions for the expression $\partial\phi(m)/\partial m$ as
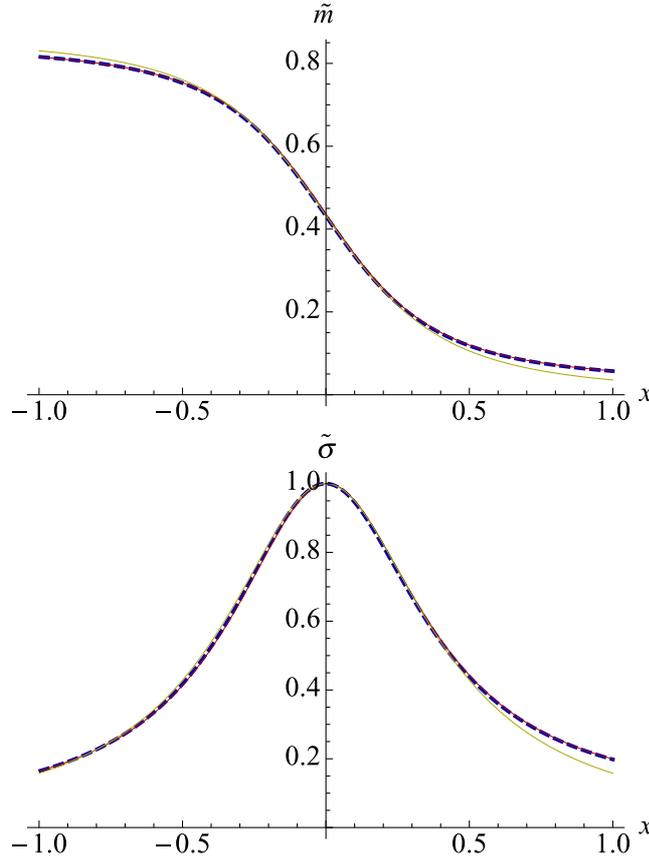
Figure 13. The scaling functions $\tilde{m}(x)$ (up) and $\tilde{\sigma}(x)$ (down) for $p = 3$ and $L = 100$. The solid red lines are the analytical results (132) and (133). The dashed blue lines are the numerical results obtained from the direct diagonalization of (109) for each x (or Γ). For (132) and (133), we need the distribution function $P_{\mathrm{P}}(m)$ and $P_{\mathrm{f}}(m)$ at $\Gamma = \Gamma_{\mathrm{c}}^{L}$. To obtain the distribution function, here, we evaluated the corresponding eigenvector for $x = 0$ (or $\Gamma = \Gamma_{\mathrm{c}}^{L}$), numerically. We also plot the infinite-size scaling functions (135) and (136) as solid yellow lines.

$$\phi(m) + \mathrm{const.} = \phi_{\pm}(m)$$

$$\equiv \int_0^m \mathrm{d}\tilde{m} \log\left[-\frac{\tilde{m}^p + e_{\mathrm{c}}^{\infty}}{(1 + \tilde{m})\Gamma_{\mathrm{c}}^{\infty}} \pm \sqrt{\left(\frac{\tilde{m}^p + e_{\mathrm{c}}^{\infty}}{(1 + \tilde{m})\Gamma_{\mathrm{c}}^{\infty}} \right)^2 - \frac{1 - \tilde{m}}{1 + \tilde{m}}} \right] \tag{141}$$

By using these two functions, we also define free energies as

$$f_{\pm}(m) \equiv \phi_{\pm}(m) + \frac{1 + m}{2} \log(1 + m) + \frac{1 - m}{2} \log(1 - m)$$

$$= \int_0^m \mathrm{d}\tilde{m} \log\left[-\frac{\tilde{m}^p + e_{\mathrm{c}}^{\infty}}{\sqrt{1 - \tilde{m}^2}\,\Gamma_{\mathrm{c}}^{\infty}} \pm \sqrt{\left(\frac{\tilde{m}^p + e_{\mathrm{c}}^{\infty}}{\sqrt{1 - \tilde{m}^2}\,\Gamma_{\mathrm{c}}^{\infty}} \right)^2 - 1} \right] \tag{142}$$

The free energy $f_{\Gamma_{\mathrm{c}}^{\infty}}(m)$ is given as the combination of $f_+(m)$ and $f_-(m)$. Here, we notice

$$f_{\Gamma_{\mathrm{c}}^{\infty}}(0) = f_{\Gamma_{\mathrm{c}}^{\infty}}(m_{\mathrm{fe}}^{\infty}) = 0. \tag{143}$$

Also, we can easily check

$$\frac{\partial f_+(m)}{\partial m}\bigg|_{m=0} > 0 \tag{144}$$

$$\frac{\partial f_-(m)}{\partial m}\bigg|_{m=0} < 0. \tag{145}$$

From (143)–(145), we can construct the free energy $f_{\Gamma_c^\infty}(m)$ as

$$f_{\Gamma_c^\infty}(m) = f_+(m) \tag{146}$$

for $m \leqslant m_c^\infty$

$$f_{\Gamma_c^\infty}(m) = f_-(m) + \text{const.} \tag{147}$$

for $m > m_c^\infty$. The constant and m_c^∞ is determined from (143) and the continuity condition

$$\lim_{m \to m_c+0} f_{\Gamma_c^\infty}(m) = \lim_{m \to m_c-0} f_{\Gamma_c^\infty}(m). \tag{148}$$

By using the parameters Γ_c^∞, e_c^∞, and m_{fe}^∞ obtained from (120)–(122), we can calculate the gap given by (138) in principle. Here, however, by using a relation

$$f_+(m) = -f_-(m) + \text{const.}, \tag{149}$$

which can be derived from the direct substitution, we will show that the gap can be expressed as a simple formula. Indeed, from this relation, we can derive

$$f_+(m_c^\infty) = \frac{1}{2}f_+(m_{\text{fe}}^\infty). \tag{150}$$

Thus, we arrive at

$$\lim_{L \to \infty} \frac{1}{L}\log \kappa = \frac{1}{2}f_+(m_{\text{fe}}^\infty)$$
$$= \int_0^{m_{\text{fe}}^\infty} \mathrm{d}m \log\left[-\frac{m^p + e_c^\infty}{\sqrt{1 - m^2\Gamma_c^\infty}} + \sqrt{\left(\frac{m^p + e_c^\infty}{\sqrt{1 - m^2\Gamma_c^\infty}}\right)^2 - 1}\right] \tag{151}$$

This formula is equivalent to the formula obtained by Bapst and Semerjian, equation (62) in reference [22]. In order to see the equivalence, we just use a basic mathematical fact that the following equations $\cosh x = A$ and $\mathrm{e}^x = A \pm \sqrt{A^2 - 1}$ are equivalent.

4. Conclusions

Our goal in this work was to identify the characteristic features of finite-size scaling at a first-order dynamical transition, as can be found generically in KCMs. As we have shown, these are akin to characteristic features of a first-order *quantum* transition. We have been able, in particular, to determine in an explicit fashion the scaling variables and the scaling functions governing the variation of the order parameter across the transition. For the

particular mean-field KCM that we have been considering here, a precise characterization of a size-dependent critical point was provided and the finite-size rounding off of the transition was fully captured by our study. Interestingly, the phenomenology of our dynamical transition—which is identical to that of quantum transitions, but now capturing finite-size scaling—also agrees with that of classical first-order transitions, as our variational formulation in terms of the mixing function $a^*(s)$ confirms.

We also note that after the submission of our work, Campostrini and collaborators presented results in a recent preprint [31] on the finite-size scaling of first-order quantum phase transition. Close to the critical point, scaling functions for their order parameter take the same form as presented in our approach, with a derivation based on a two-level effective model. Further connections between our work and this approach (and also with the two-level effective model of [21] used for an instantonic computation of the gap) are worth studying.

The mean-field version being now fully understood, a more challenging program awaits ahead of us. Finite-dimensional systems of course display a richer phenomenology [13] with, for instance, the existence of surface tension and nucleating droplets. It is in principle possible to extend our analysis for the density large deviation function to a space varying field, by means of field theoretic methods à la Doi–Peliti [32, 33], for example. When studying dynamical transitions, some authors [10] work at fixed system size, but they perform a finite time analysis (which would be mimicked by a finite temperature analysis in quantum phase transition). It would certainly be of interest to quantify in a similar way finite time corrections, though the phase transition itself is indeed a collective effect captured only at large N. These issues are currently under investigation.

Acknowledgments

Appendix A. Determination of s_c

In this appendix, we derive $s_c = 1/(2Lc(1-c)) + O(1/L^2)$. We evaluate (87) up to $O(1/L)$ by using the explicit expressions of r, $\tilde{r}_i$, and $\tilde{r}_a$. From a saddle point approximation, we rewrite the left-hand side of (87) as

$$\frac{1}{L}\left(\tilde{r}_i e^{-s_c} - r\right)\Big|_{n=1} + O(1/L^2) = \frac{c}{L}e^{-s_c}\frac{e^{-Lf_i(2/L)/2}}{e^{-Lf_i(1/L)/2}} - \frac{c}{L} + O(1/L^2). \quad (A.1)$$

Here, the first term is $O(1/L^2)$ since

$$\frac{e^{-Lf_i(2/L)/2}}{e^{-Lf_i(1/L)/2}} = O(1/L). \quad (A.2)$$

Thus, the left-hand side of (87) is $-c/L + O(1/L^2)$. On the other hand, the right-hand side of (87) is evaluated by a saddle point approximation as

$$
\frac{1}{L}\left(\tilde{r}_{\mathrm{a}}\mathrm{e}^{-s_{\mathrm{c}}} - r\right)\Big|_{n=Lc} + O(1/L^2)
$$
$$
= c^2(1-c)\left[\mathrm{e}^{-\frac{1}{2}\frac{\partial f_a(\rho)}{\partial \rho}|_{\rho=c} - s_{\mathrm{c}}} + \mathrm{e}^{\frac{1}{2}\frac{\partial f_a(\rho)}{\partial \rho}|_{\rho=c} - s_{\mathrm{c}}} - 2\right] + O(1/L^2). \quad \text{(A.3)}
$$

By noticing that $\partial f_a(\rho)/\partial \rho|_{\rho=c}$ and s_{c} are $O(1/L)$, we rewrite (A.3) as

$$
-2s_{\mathrm{c}}\,c^2(1-c) + O(1/L^2). \quad \text{(A.4)}
$$

Therefore, by equating the left-hand side of (87) to the right-hand side of (87), we arrive at

$$
s_{\mathrm{c}} = \frac{1}{2Lc(1-c)} + O(1/L^2). \quad \text{(A.5)}
$$

Appendix B. Finite-size corrections to the free energy difference

In this appendix, we derive the finite-size correction $\Delta f_{s_{\mathrm{c}}}^{(1)}(\rho)$ given in (39) and (40). We first focus on the region $\rho > \rho_{\mathrm{c}}^L$. From (26) with (38), we find that $\Phi_{\mathrm{L}}(n)$ doesn't satisfy the large deviation principle. Then, we define $\tilde{\Phi}_{\mathrm{L}}(\rho) = \Phi_{\mathrm{L}}(\rho L)$. From the fact $\Phi_{\mathrm{L}}(n)$ doesn't satisfy the large deviation scaling, we can assume $\tilde{\Phi}_{\mathrm{L}}(\rho)$ is differentiable:

$$
\tilde{\Phi}_{\mathrm{L}}(\rho \pm 1/L) = \tilde{\Phi}_{\mathrm{L}}(\rho) \pm \frac{\partial \tilde{\Phi}_{\mathrm{L}}}{\partial \rho}\frac{1}{L} + O(1/L^2). \quad \text{(B.1)}
$$

By rewriting the left-hand side of (26) using this scaling, we obtain a differential equation for determining $\tilde{\Phi}_{\mathrm{L}}(\rho)$.

$$
\tilde{\Phi}_{\mathrm{L}}(\rho)\left\{-\tilde{s}_c\rho\left[c + (1-2c)\rho\right] + c\right\} + \frac{\partial \tilde{\Phi}_{\mathrm{L}}(\rho)}{\partial \rho}\rho(c-\rho) + O(1/L^2) = 0, \quad \text{(B.2)}
$$

where we defined $\tilde{s}_c \equiv sL$. By solving this differential equation, we obtain

$$
-2\log\tilde{\Phi}_{\mathrm{L}}(\rho) = -2\left[\tilde{s}_c\rho(2c-1) - \log\rho + (-\tilde{s}_c 2c(1-c) + 1)\log|c-\rho|\right] + \text{const.} \quad \text{(B.3)}
$$

Finally with a relation $\tilde{s}_c = 1/(2c(1-c)) + O(1/L)$, we can omit the last term. The result leads to

$$
-2\log\tilde{\Phi}_{\mathrm{L}}(\rho) = \Delta f_{s_c}^{(1)}(\rho) = -2\left[\frac{\rho(2c-1)}{2c(1-c)} - \log\rho\right] + \text{const.} \quad \text{(B.4)}
$$

Next, we focus on the region $\rho \leqslant \rho_{\mathrm{c}}^L$. By using the explicit expression of $\Delta f_{s_{\mathrm{c}}}$ in this region, we evaluate the equation (26) up to $O(1/L)$. First, $\Phi_{\mathrm{L}}(n+1)/\Phi_{\mathrm{L}}(n)$ is evaluated as

$$
\frac{\Phi_{\mathrm{L}}(n+1)}{\Phi_{\mathrm{L}}(n)} = \mathrm{e}^{\partial f_{\mathrm{e}}/\partial \rho + 1/(2L)\partial^2 f_{\mathrm{e}}/\partial \rho^2 - 1/(2L)\partial\Delta f_{sc}^{(1)}/\partial \rho}
$$
$$
= \frac{(1-c)\rho}{c(1-\rho)}\mathrm{e}^{(1/(2L\rho(1-\rho)))}\mathrm{e}^{-1/(2L)\partial\Delta f_{sc}^{(1)}/\partial \rho}. \quad \text{(B.5)}
$$

Then, we obtain an equation for determining $\Delta f_{s_c}^{(1)}$ as

$$
\begin{aligned}
\frac{\partial \Delta f_{s_c}^{(1)}(\rho)}{\partial \rho} &= \frac{2}{\rho} - 2 \frac{\frac{c}{\rho} + [(1-c)\rho + c(1-\rho)]\left[\frac{1}{2\rho(1-\rho)} - \frac{1}{2c(1-c)}\right]}{-(1-c)\rho + c(1-\rho)} \\
&= -\frac{1}{\rho} + \frac{1}{1-\rho} - \frac{2}{c-\rho} - \frac{1-2c}{c(1-c)},
\end{aligned}
\tag{B.6}
$$

which leads to

$$
\Delta f_{s_c}^{(1)}(\rho) = -\log \frac{\rho(1-\rho)}{(c-\rho)^2} - \frac{\rho(1-2c)}{c(1-c)} + \text{const.}
\tag{B.7}
$$

Appendix C. Table of notations

Quantity	Notation	Defining equation
Transition rates	$w(n \to n')$	(1)
Equilibrium distribution	$P_{\text{eq}}(n)$	(5)
Equilibrium free energy	$f_{\text{e}}(\rho)$	(6)
Dynamical free energy or cumulant generating function	$\psi(s)$	(7)
Matrix of evolution	W	(9)
Left eigenvector of W for the eigenvalue $L\psi(s)$	Φ_{L}	(8)
Transition rates of the modified dynamics	$w_s(n \to n')$	(14)
Equilibrium distribution for the modified dynamics	$P^s(n)$	(15)
Free energy difference	$\Delta F_s(n)$	(16)
Finite-size critical point	s_{c}	(17)
Scaled critical point	λ_{c}	(18)
Rescaled dynamical free energy	$\varphi_L(\lambda)$	(22)
Density of free energy difference	$\Delta f_{\text{s}}(\rho)$	(27)
Infinite-size connecting point	ρ_{c}^{∞}	(36)
Finite-size connecting point	ρ_{c}^L	(37)
First-order correction (in powers of L) to $\Delta f_{\text{s}}(\rho)$	$\Delta f_{\text{s}}^{(1)}(\rho)$	(38)
Mean occupation number	$\rho(s)$	(41)
Variance of the occupation number	$\chi(s)$	(42)
Scaling ratio	κ	(43)
Scaling variable	x	(44)
Rescaled $\rho(s)$	$\tilde{\rho}(x)$	(45)
Rescaled $\chi(s)$	$\tilde{\chi}(x)$	(46)
Variational function for determining Φ_L	$\tilde{\Phi}_{\text{L}}(n)$	(47)
Variational distribution	$\widetilde{P}(n)$	(49)
Variational function for the free energy difference	$\Delta\widetilde{F}(n)$	(50)
Variational function for the density of free energy difference	$\tilde{f}(\rho)$	(53)
Finite-size free energy difference in inactive region	$f_{\text{i}}(\rho)$	(59)
Finite-size free energy difference in active region	$f_{\text{a}}(\rho)$	(60)
Distribution in inactive region at the transition point	$P_{\text{i}}(n)$	(62)
Distribution in active region at the transition point	$P_{\text{a}}(n)$	(63)
Mixing function	$a^*(s)$	(66)

(*Continued*)

Quantity	Notation	Defining equation
Variational function with mixing parameter a	$\Psi(a)$	(70)
Infinite-size scaling function of $\tilde{\rho}(x)$	$\tilde{\rho}_\infty(x)$	(94)
Infinite-size scaling function of $\tilde{\chi}(x)$	$\tilde{\chi}_\infty(x)$	(95)
Hamiltonian of the mean-field p-spin ferromagnet	$\hat{H}$	(105)
Distribution of magnetization with transverse field Γ	$p^\Gamma(m)$	(112)
Eigenvector of the Hamiltonian with interchange symmetry	$\Phi(m^z)$	(106)
Number of the state	$p(m)$	(110)
Ground state mean magnetization with transverse field Γ	$m(\Gamma)$	(113)
Ground state susceptibility with transverse field Γ	$\sigma(\Gamma)$	(114)
Transverse field at the transition point in infinite-size limit	Γ_c^∞	(122)
Ground state mean magnetization at $\Gamma = \Gamma_c^\infty$ in infinite-size limit	m_∞^{fe}	(122)
Transverse field at the transition point for a finite-size system	Γ_c^L	(123)
Rescaled $m(\Gamma)$	$\tilde{m}(x)$	(124)
Rescaled $\sigma(\Gamma)$	$\tilde{\sigma}(x)$	(125)
Finite-size connecting point	m_c	(126)
Mixing function for the case of quantum ferromagnet	$a^*(\Gamma)$	(128)
Infinite-size scaling function for $\tilde{m}(x)$	$\tilde{m}_\infty(x)$	(135)
Infinite-size scaling function for $\tilde{\sigma}(x)$	$\tilde{\sigma}_\infty(x)$	(136)
Free energy density for the quantum ferromagnet	$f_\Gamma(m)$	(137)
Infinite-size connecting point	m_c^∞	(138)
Mean energy density for the ground state at $\Gamma = \Gamma_c^\infty$	e_c^∞	(140)

References

[1] Ritort F and Sollich P 2003 Glassy dynamics of kinetically constrained models *Adv. Phys.* **52** 219
[2] Garrahan J P, Sollich P and Toninelli C 2011 Dynamical heterogeneities and kinetically constrained models *Dynamical Heterogeneities in Glasses, Colloids, and Granular Media* ed L Berthier *et al* (Oxford: Oxford University Press)
[3] Ruelle D 2004 *Thermodynamic Formalism: the Mathematical Structures of Equilibrium Statistical Mechanics* 2nd edn (Cambridge: Cambridge University Press)
[4] Sinai Y G 1972 Gibbs measures in ergodic theory *Russ. Math. Surveys* **27** 21
[5] Bowen R 2008 *Equilibrium States and the Ergodic Theory of Anosov Diffeomorphisms* (*Lecture Notes in Mathematics* vol 470) 2nd edn (Berlin: Springer)
[6] Lecomte V, Appert-Rolland C and van Wijland F 2005 Chaotic properties of systems with Markov dynamics *Phys. Rev. Lett.* **95** 010601
[7] Merolle M, Garrahan J P and Chandler D 2005 Space-time thermodynamics of the glass transition *Proc. Natl Acad. Sci.* **102** 10837
[8] Garrahan J P, Jack R L, Lecomte V, Pitard E, van Duijvendijk K and van Wijland F 2007 Dynamical first-order phase transition in kinetically constrained models of glasses *Phys. Rev. Lett.* **98** 195702
[9] Garrahan J P, Jack R L, Lecomte V, Pitard E, van Duijvendijk K and van Wijland F 2009 First-order dynamical phase transition in models of glasses: an approach based on ensembles of histories *J. Phys. A: Math. Theor.* **42** 075007
[10] Hedges L O, Jack R L, Garrahan J P and Chandler D 2009 Dynamic order-disorder in atomistic models of structural glass formers *Science* **323** 1309
[11] Pitard E, Lecomte V and Van Wijland F 2011 Dynamic transition in an atomic glass former: a molecular dynamics evidence *Europhys. Lett.* **96** 56002
[12] Whitelam S and Garrahan J P 2004 Geometrical picture of dynamical facilitation *J. Phys. Chem.* B **108** 6611
[13] Bodineau T and Toninelli C 2012 Activity phase transition for constrained dynamics *Commun. Math. Phys.* **311** 357
[14] Bodineau T, Lecomte V and Toninelli C 2012 Finite size scaling of the dynamical free-energy in a kinetically constrained model *J. Stat. Phys.* **147** 1
[15] Lecomte V, Garrahan J P and van Wijland F 2012 Inactive dynamical phase of a symmetric exclusion process on a ring *J. Phys. A: Math. Theor.* **45** 175001

[16] Borgs C and Kotecký R 1990 A rigorous theory of finite-size scaling at first-order phase transitions *J. Stat. Phys.* **61** 79

[17] Borgs C and Kotecký R 1992 Finite-size effects at asymmetric first-order phase transitions *Phys. Rev. Lett.* **68** 1734

[18] Privman V and Fisher M E 1983 Finite-size effects at first-order transitions *J. Stat. Phys.* **33** 385

[19] van Kampen N G 2007 *Stochastic Processes in Physics and Chemistry* (Amsterdam: North Holland)

[20] Parisi G 1988 *Statistical Field Theory* (Reading, MA: Addison-Wesley)

[21] Jörg T, Krzakala F, Kurchan J, Maggs A C and Pujos J 2010 Energy gaps in quantum first-order mean-field–like transitions: the problems that quantum annealing cannot solve *Europhys. Lett.* **89** 40004

[22] Bapst V and Semerjian G 2012 On quantum mean-field models and their quantum annealing *J. Stat. Mech.* P06007

[23] Derrida B and Lebowitz J L 1998 Exact large deviation function in the asymmetric exclusion process *Phys. Rev. Lett.* **80** 209

[24] Lecomte V, Appert-Rolland C and van Wijland F 2007 Thermodynamic formalism for systems with markov dynamics *J. Stat. Phys.* **127** 51

[25] Giardinà C, Kurchan J and Peliti L 2006 Direct evaluation of large-deviation functions *Phys. Rev. Lett.* **96** 120603

[26] Lecomte V and Tailleur J 2007 A numerical approach to large deviations in continuous time *J. Stat. Mech.* P03004

[27] Giardinà C, Kurchan J, Lecomte V and Tailleur J 2011 Simulating rare events in dynamical processes *J. Stat. Phys.* **145** 787

[28] Nemoto T and Sasa S i 2011 Variational formula for experimental determination of high-order correlations of current fluctuations in driven systems *Phys. Rev.* E **83** 030105

[29] Nemoto T and Sasa S I 2011 Thermodynamic formula for the cumulant generating function of time-averaged current *Phys. Rev.* E **84** 061113

[30] Jack R L and Sollich P 2010 Large deviations and ensembles of trajectories in stochastic models *Prog. Theor. Phys. Suppl.* **184** 304

[31] Campostrini M, Pelissetto A and Vicari E 2014 Finite-size scaling at quantum transitions *Phys. Rev.* B **89** 094516

[32] Doi M 1976 Second quantization representation for classical many-particle system *J. Phys. A: Math. Gen.* **9** 1465

[33] Peliti L 1985 Path integral approach to birth-death processes on a lattice *J. Phys. France* **46** 1469